Title:

Biosynthesis of gibberellin-related compounds modulates far-red light responses in the liverwort *Marchantia polymorpha*

Authors:

Rui Sun (孙 芮)[1], Maiko Okabe (岡部 麻衣子)[1], Sho Miyazaki (宮崎 翔)[2], Toshiaki Ishida (石田 俊晃)[3], Kiyoshi Mashiguchi (増口 潔)[3], Keisuke Inoue (井上 佳祐)[1], Yoshihiro Yoshitake (吉竹 良洋)[1], Shohei Yamaoka (山岡尚平)[1], Ryuichi Nishihama (西浜 竜一)[1,4], Hiroshi Kawaide (川出 洋)[5], Masatoshi Nakajima (中嶋 正敏)[6], Shinjiro Yamaguchi (山口 信次郎)[3], Takayuki Kohchi (河内 孝之)[1,*]

[1] Graduate School of Biostudies, Kyoto University, Kyoto 606-8502, Japan.

[2] Institute of Global Innovation Research, Tokyo University of Agriculture and Technology, Fuchu, 183-8509, Japan.

[3] Institute for Chemical Research, Kyoto University, Uji 611-0011, Japan.

[4] Department of Applied Biological Science, Faculty of Science and Technology, Tokyo University of Science, Noda 278-8510, Japan.

[5] Institute of Agriculture, Tokyo University of Agriculture and Technology, Tokyo 183-8509, Japan.

[6] Department of Applied Biological Chemistry, The University of Tokyo, Tokyo 113-8657, Japan.

[*] Correspondence: tkohchi@lif.kyoto-u.ac.jp

Short title:

GA biosynthesis in *M. polymorpha*

The author responsible for distribution of materials integral to the findings presented in this article in accordance with the policy described in the Instructions for Authors (https://academic.oup.com/plcell/pages/General-Instructions) is: Takayuki Kohchi (tkohchi@lif.kyoto-u.ac.jp).

ABSTRACT

The phytohormone gibberellins (GAs) are key regulators of growth, development and environmental responses in angiosperms. From an evolutionary perspective, all major steps of GA biosynthesis are conserved among vascular plants, while GA biosynthetic intermediates such as *ent*-kaurenoic acid (KA) are also produced by bryophytes. Here we show that in the liverwort *Marchantia polymorpha*, KA and GA_{12} are synthesized by evolutionarily conserved enzymes, which are required for developmental responses to far-red light (FR). Under FR-enriched conditions, mutants of various biosynthesis enzymes consistently altered thallus growth allometry, delayed the initiation of gametogenesis, and affected the morphology of gamete-bearing structures (gametangiophores). By chemical treatments and LC-MS/MS analyses, we confirmed these phenotypes were caused by deficiency of some GA-related compounds derived from KA, but not bioactive GAs from vascular plants. Transcriptome analysis showed that FR enrichment induced the up-regulation of genes related to stress responses and secondary metabolism in *M. polymorpha*, which was largely dependent on the biosynthesis of GA-related compounds. Due to the lack of the canonical GA receptors in bryophytes, we hypothesize that GA-related compounds are commonly synthesized in land plants but co-opted independently to regulate responses to light quality change in different lineages during the past 450 million years of evolution.

INTRODUCTION

Throughout evolution, plants developed various chemical tools to optimize growth and development, and to cope with environmental changes. Gibberellins (GAs) are a group of tetracyclic diterpenoid compounds broadly produced by many plants and plant-associated microbes. Among the more than 130 identified GAs, a few of them (GA_1, GA_3, GA_4, and GA_7) are considered as commonly bioactive in angiosperms (reviewed in Sponsel, 2016), stimulating seed germination (Koornneef and van der Veen, 1980; Toyomasu et al., 1998; Yamaguchi et al., 1998a; Ogawa et al., 2003; Gabriele et al., 2009) and promoting growth of various plant organs (Kurosawa, 1926; Koornneef and van der Veen, 1980; Wenzel et al., 2000; Ubeda-Tomás et al., 2008, 2009; Achard et al., 2009; Nelissen et al., 2012).

In *Arabidopsis thaliana*, the biosynthesis of GAs starts with the production of *ent*-kaurene from geranylgeranyl diphosphate (GGDP) by two terpene synthases (TPSs), *ent*-copalyl diphosphate

synthase (CPS) and *ent*-kaurene synthase (KS) (Sun and Kamiya, 1994; Yamaguchi et al., 1998b). Next, *ent*-kaurene is oxidized by two cytochrome P450 monooxygenases (CYPs), first into *ent*-kaurenoic acid (KA) by *ent*-kaurene oxidase (KO), then into GA_{12} by *ent*-kaurenoic acid oxidase (KAO) (Helliwell et al., 1998, 1999, 2001a, 2001b). Finally, GA_{12} is converted into the bioactive form GA_4 through sequential oxidation by two 2-oxoglutarate-dependent dioxygenases (2-OGDs), GA 20-oxidase (GA20ox) and GA 3-oxidase (GA3ox) (Chiang et al., 1995; Yamaguchi et al., 1998a; Williams et al., 1998). A second bioactive GA, GA_1, is different from GA_4 by one additional hydroxyl group on C-13, which is possibly introduced to GA_{12} or KA before the subsequent oxidation steps (Talon et al., 1990; Nomura et al., 2013) (Supplemental Figure 1).

Bioinformatic and chemical analyses revealed that this biosynthetic pathway producing GA_4 and/or GA_1 is conserved among vascular plants (Hirano et al., 2007; Tanaka et al., 2014; Cannell et al., 2020). In several fern species, GA-derived compounds modulate sexual differentiation of gametophytes and spore germination in the darkness (Yamane, 1998; Schneller, 2008; Tanaka et al., 2014; Hornych et al., 2021). Bryophytes have no 2-OGD-family members of GA biosynthesis enzymes, thus considered as lacking the production of common bioactive GAs. However, homologs for CPS, KS, KO and KAO still exist in bryophytes, which suggested an ancestral capacity to synthesize the GA precursors KA and GA_{12} in all land plants (Cannell et al., 2020). In the moss *Physcomitrium patens* which lacks KAO, KA is synthesized by a bifunctional CPS/KS and a single KO homolog (Hayashi et al., 2006, 2010; Miyazaki et al., 2011, 2015). The KA derivative, *ent*-3β-OH-KA, is known as a bioactive molecule to regulate protonema differentiation and blue light avoidance in *P. patens* (Hayashi et al., 2010; Miyazaki et al., 2014, 2015, 2018).

In the liverwort *Marchantia polymorpha*, homologs for CPS, KS, KO and KAO were identified in genome-wide analyses (Kumar et al., 2016; Bowman et al., 2017). Also, MpCPS/DTPS3 and MpKS/DTPS4 (hereafter referred to as MpCPS and MpKS) have been reported to catalyze the production of *ent*-copalyl diphosphate and *ent*-kaurene (Kumar et al., 2016; Jia et al., 2022). In transcriptome analysis, upregulation of GA biosynthesis gene homologs was observed under far-red light (FR) enriched conditions, suggesting a role for this pathway in the response to light quality change (Briginshaw et al., 2022). However, no empirical knowledge has been established yet about the exact physiological function of GA-related compounds in liverworts.

FR enrichment mimics the proximity of competitive neighbors in the nature habitat. In many angiosperms, this is perceived by phytochrome (phy) photoreceptors and triggers shade-avoiding responses, including elongation of stem-like structures, hyponastic growth of petioles and acceleration of flowering (Downs et al., 1957; Holmes and Smith, 1975; Morgan and Smith, 1978, 1979; Whitelam and Johnson, 1982; Whitelam and Smith, 1991). GA biosynthesis is often evoked in this process, and is required for the induction of elongative growth (García-Martínez et al., 1987; Beall et al., 1996; Van Tuinen et al., 1999; Hisamatsu et al., 2005; Djakovic-Petrovic et al., 2007; Dubois et al., 2010). For example, in *A. thaliana*, a local FR enrichment at the leaf tip induced the expression of GA biosynthesis genes in both the leaf tip and the petiole, which modulates the hyponastic growth of the petiole (Sessa et al., 2005; Hisamatsu et al., 2005; Djakovic-Petrovic et al., 2007; Bou-Torrent et al., 2014; Kohnen et al., 2016; Küpers et al., 2023). In the gymnosperm *Pinus tabuliformis*, FR-induced shoot elongation was also accompanied with and dependent on the accumulation of bioactive GAs (Li et al., 2020).

As a liverwort, the life cycle of *M. polymorpha* is dominated by the thalloid gametophyte. End-of-day FR irradiation is known to cause hyponastic growth of thallus tips and decrease in chlorophyll (Fredericq, 1964; Ninnemann and Halbsguth, 1965; Fredericq and de Greef, 1966; Fredericq and Greef, 1968). FR enrichment also induced hyponastic thallus growth (Briginshaw et al., 2022), accompanied by the growth activity change of apical meristems and the transition to sexual reproduction (Chiyoda et al., 2008; Inoue et al., 2019; Streubel et al., 2023). Similar to *A. thaliana* and other land plants, these responses in *M. polymorpha* are mediated by the sole phytochrome (Mpphy) and the single-copy transcription factor PHYTOCHROME-INTERACTING FACTOR (MpPIF) (Fredericq, 1964; Inoue et al., 2016, 2019; Streubel et al., 2023). In this study, we characterized evolutionarily conserved GA biosynthesis enzymes in *M. polymorpha* with genetic approach, showing that they were indispensable for developmental and gene expression responses to FR enrichment.

RESULTS

Mp*CPS* is required for thallus morphological changes induced by FR enrichment

To explore the function of GA-related hormones in *M. polymorpha*, we used the CRISPR/Cas9^{D10A} nickase system (Hisanaga et al., 2019; Koide et al., 2020) to create large-deletion mutants of Mp*CPS* (Mp2g07200), which encodes the first enzyme of the biosynthesis

120 pathway. Two different mutant alleles (Mp*cps-4*^{ld} and Mp*cps-27*^{ld}) with complete loss of the
121 coding sequence (CDS) were isolated from Tak-1, a male wild-type accession (Supplemental
122 Figure 2A). Mp*cps-4*^{ld} was further complemented by expressing the CDS of Mp*CPS* with C-
123 terminal Citrine fusion under the control of a cauliflower mosaic virus 35S promoter
124 ($_{pro}$*35S:*Mp*CPS-Cit*), generating two independent transgenic lines. First, we observed the thallus
125 morphology of 12-day-old plants grown from gemmae under two different light conditions, either
126 the continuous white light (cW), or cW supplemented with continuous far-red light (cW+cFR). FR
127 enrichment under cW+cFR induced morphological changes in Tak-1 wild-type plants, marked
128 by increased growth angles (hyponasty) and slenderer thallus shapes, the latter shown as the
129 increase of length-width ratio measured from half of the thallus (Figure 1A-C). Such an increase
130 was not observed in Mp*cps*^{ld} mutants, suggesting a role for Mp*CPS* in modulating FR-induced
131 growth responses. Furthermore, Mp*cps*^{ld} mutants were significantly larger in thallus size than
132 wild-type plants, particularly under cW+cFR conditions (Figure 1A,D). It is likely that MpCPS acts
133 in a pathway producing compounds inhibiting growth, rather than promoting growth like bioactive
134 GAs in angiosperms. The complementation lines carrying $_{pro}$*35S:*Mp*CPS-Cit* recovered the
135 hyponastic growth, the thallus shape and the thallus size of Mp*cps-4*^{ld}, confirming that the
136 phenotypes were caused by Mp*CPS* loss-of-function (Figure 1A-D). As a further verification,
137 Mp*cps*^{ld} mutant alleles and complementation lines were constructed in the female wild-type
138 accession (Tak-2). Similarly, Mp*cps*^{ld} mutations resulted in decrease of thallus hyponasty and
139 the length-width ratio, but increased the thallus area drastically under cW+cFR (Supplemental
140 Figure 3).

141 To examine the influence of Mp*cps*^{ld} on growth activity at the tissue level, we labelled 7-day-
142 old plants grown under cW+cFR with 5-ethynyl-2'-deoxyuridine (EdU), which could be
143 incorporated into actively dividing cells during DNA synthesis. In the wild-type plants, we
144 observed a relatively narrow distribution of EdU-positive nuclei in the slender thallus, dispersing
145 from the apical meristem to the basal region along the midrib. By assigning different pseudo-
146 colors to signals acquired at different depths by confocal microscopy, we found different
147 distributions of dorsal and ventral signals in these plants. Ventral EdU signals along the midrib
148 extended further in the basal direction, suggesting excessive cell divisions specific to the ventral
149 side, which might contribute to the hyponastic growth induced by FR enrichment (Figure 1E).
150 While in Mp*cps*^{ld} mutants, EdU signals indicated active cell divisions in a broader range. Two

151 fully separated apical meristems were usually seen from the observed region, and the total
152 numbers of EdU-positive nuclei were significantly higher than those of wild-type plants or
153 complementation lines (Figure 1E-F). In addition, dorsal and ventral EdU signals showed similar
154 distribution ranges in Mp*cps*^{ld} mutants, which was consistent with their flat morphology under
155 cW+cFR (Figure 1E).
156

157 **Mp*CPS* has a role in modulating gametangiophore development**

158 Continuous FR irradiation is known to induce sexual reproduction in *M. polymorpha*, i.e. the
159 formation of sexual branches called gametangiophores, and the differentiation of sexual organs
160 called gametangia (Yamaoka et al., 2018; Inoue et al., 2019). To observe this process, plants
161 were grown from gemmae under cW for 7 days, then transferred to cW+cFR for
162 gametangiophore induction. As a liverwort, *M. polymorpha* undergoes vegetative growth with
163 dichotomous branching, periodically multiplying the number of apical meristems through
164 bifurcation. Generally, all apical meristems remain indeterminate under white light conditions,
165 while a proportion of them become dormant or differentiate into gametangiophores under FR-
166 enriched light conditions (Streubel et al., 2023). During the induction under cW+cFR, we
167 observed higher numbers of total apical meristems in Mp*cps*^{ld} mutants than in wild-type or
168 complementation lines, which is in line with their more active vegetative growth (Figure 2A-B;
169 Supplemental Figure 4A). If the potential for apical meristems to form gametangiophores was
170 similar between the mutants and wild-type plants, higher number of gametangiophore-bearing
171 apexes would be expected in Mp*cps*^{ld} mutants. However, Mp*cps*^{ld} mutants formed fewer
172 gametangiophores than wild-type plants and complementation lines during the first 16 days after
173 FR irradiation, suggesting that gametangiophore formation is inhibited in these mutants (Figure
174 2A-B; Supplemental Figure 4A).

175 In addition, the morphology of gametangiophores was distorted in Mp*cps*^{ld} mutants. As *M.*
176 *polymorpha* is a dioicous species, gametangiophores are sexually dimorphic among plants with
177 different sex chromosomes. The male gametangiophores (antheridiophores) of wild-type plants
178 had roundish, disc-like receptacles, which were ventrally connected to a relatively long and thin
179 stalk at the center. While for Mp*cps*^{ld} mutants, the male receptacles were fan-shaped, attaching
180 to a short and thick stalk(s) at the basal end (Fig 2C,E; Supplemental Figure 4B). Transverse
181 sectioning revealed thallus-like features in the stalks of Mp*cps*^{ld} antheridiophores. Usually, no

182 air chambers could be observed in the near-cylindric antheridiophore stalks of wild-type plants.
183 In contrast, Mp*cps*^{ld} antheridiophore stalks had a flat dorsal surface beneath which air chambers
184 with photosynthetic filaments were clearly formed (Supplemental Figure 5A), quite similar to the
185 tissue organization in the vegetative thallus (Shimamura, 2016). Besides, Mp*cps*^{ld}
186 antheridiophore stalks frequently have more canals with pegged rhizoids in the ventral side,
187 possibly reflecting additional bifurcation events during gametangiophore morphogenesis
188 (Supplemental Figure 5A).

189 The female gametangiophores (archegoniophores) of wild-type plants were also stalked and
190 had 9-11 finger-like structure (digitate rays) in the receptacle, which radially arranged like
191 umbrella ribs. Two marginal digitate rays could be recognized as no involucres were produced
192 between them (Figure 2D,F; Supplemental Figure 4B) (Cao et al., 2013). The female receptacles
193 of Mp*cps*^{ld} were palm-like, positioning the two marginal rays at opposite ends. Excessive number
194 of digitate rays and/or bifurcation in the stalk were often observed in late-stage receptacles
195 (Figure 2D,F; Supplemental Figure 4B). In extreme cases from aseptic culture, the
196 archegoniophore of Mp*cps*^{ld} remained the form of bifurcated thalloid branches, with digitate rays
197 formed at the thallus tips (Supplemental Figure 4C). If the relatively fixed number of digitate rays
198 in wild-type receptacles represents a determinate fate for the apical meristem, such excessive
199 bifurcation or additional digitate rays in Mp*cps*^{ld} mutants might suggest a loose transition from
200 the indeterminate vegetative growth. Similar to the male case, the stalks of Mp*cps*^{ld}
201 archegoniophores were shorter and thicker than the wild-type counterparts, bearing more rhizoid
202 canals in the ventral side (Figure 2D; Supplemental Figure 5C).

203 Since gametangium differentiation accompanies the morphogenesis of gametangiophores,
204 we investigated this progress by examining Citrine-labelled MpBONOBO proteins (MpBNB-Cit),
205 which specifically accumulate in the initial cells and immature gametangia (Yamaoka et al., 2018).
206 To keep the consistency in genetic background, large-deletions of Mp*CPS* were introduced into
207 Mp*BNB-Cit* knock-in lines through thallus transformation (Supplemental Figure 2), again using
208 the CRISPR/Cas9^{D10A} nickase system (Hisanaga et al., 2019). As expected, the
209 gametangiophore morphogenesis was delayed by Mp*cps*^{ld} mutation. After 11 or 14 days of
210 growth under cW+cFR, dome-shaped gametangiophore primordia already formed, respectively,
211 in male and female Mp*BNB-Cit* plants carrying the wild-type Mp*CPS* allele. Under fluorescence
212 microscopes, arrays and/or clusters of Citrine signals appeared at the edge of primordia,

213 indicating on-going gametangium differentiation in these plants. In contrast, no gametangiophore
214 primordium was yet visible in Mp*cps*^{ld} Mp*BNB-Cit* lines of the same ages. Few or no Citrine-
215 positive nuclei could be found in the apical regions of these plants, suggesting that Mp*cps*^{ld} also
216 caused a delay in gametangium differentiation (Figure 2G-J). Despite such delay, male and
217 female gametangia of normal morphology eventually formed in Mp*cps*^{ld} mutants, as shown by
218 the longitudinal sections of the receptacles (Supplemental Figure 5B,D). Crossing experiments
219 further confirmed the fertility of gametes, as mature spores could be produced from all
220 combinations among Mp*cps*^{ld} and wild-type plants (Supplemental Figure 5E-F).
221

222 **Mp*cps*^{ld} phenotypes can be rescued by *ent*-kaurenoic acid (KA)**

223 To explore the GA biosynthesis pathway possibly blocked by Mp*cps*^{ld}, we first investigated if
224 common GAs from angiosperms could be detected endogenously in *M. polymorpha*. The plants
225 were cultured for 10 days under cW, then 4 days under cW+cFR before harvested for analysis
226 with liquid chromatography-tandem mass spectrometry (LC-MS/MS). In the Tak-1 wild-type
227 plants, GA_{12} but not any downstream compounds from the angiosperm GA biosynthesis pathway
228 could be detected (Figure 3A-B; Supplemental Figures 1 and 6A). The endogenous level of GA_{12}
229 is 28.9 ± 6.5 pg/g fresh weight on average, which is much lower than the levels in the seedlings
230 of *Arabidopsis thaliana* (Nomura et al., 2013). In Mp*cps-4*^{ld} plants cultured under the same
231 conditions, endogenous GA_{12} did not reach the detection limit, which supported the loss of GA
232 biosynthesis in this mutant (Figure 3B).

233 Next, we tested the effect of GA-related compounds on *M. polymorpha*. For thallus
234 morphology observation, gemmae were planted on agar medium containing different GAs or the
235 solvent control, then cultured under cW+cFR for 12 days. For gametangiophore induction, plants
236 were transferred onto agar medium containing chemicals at the onset of cW+cFR induction.
237 Several bioactive GAs in vascular plants and the GA biosynthesis precursor, KA, were tested on
238 wild-type and Mp*cps-4*^{ld} mutants. GA_{12} was not included in the assay due to its limited availability.
239 As a result, 2-μM KA application fully complemented Mp*cps-4*^{ld} phenotypes. The thallus shape,
240 the progress of gametangiophore formation and the gametangiophore morphology were all
241 restored to the manner of wild-type plants (Figure 3C-F). Furthermore, KA treatment altered the
242 thallus morphology of Mp*cps-4*^{ld} in a dose-dependent manner under cW+cFR. 100-nM KA was
243 sufficient to induce clear changes in the size, shape and hyponasty of the mutant thallus

244 (Supplemental Figure 7A, C-E). However, KA did not evidently change the thallus shape or
245 gametangiophore formation in wild-type plants, which suggested it to be a biosynthetic
246 intermediate rather than being directly bioactive. No active GAs in angiosperms (GA_1, GA_3 or
247 GA_4) rescued Mp*cps-4*^{ld} as efficiently as KA, which was consistent with their absence in *M.*
248 *polymorpha*. GA_9 methyl ester (GA_9-Me), which is released by several ferns as a pheromone
249 and could rescue Pp*cps/ks* phenotype in the moss *P. patens* (Yamauchi et al., 1996; Tanaka et
250 al., 2014; Hayashi et al., 2010), did not work on Mp*cps-4*^{ld} in *M. polymorpha* (Figure 3C-F).
251 Taken together, these data indicated that Mp*cps*^{ld} phenotypes were likely caused by the
252 deficiency in some GA-related diterpenoid compound(s), which is synthesized from KA but
253 different from bioactive GAs in vascular plants. For convenience, hereafter we refer to this
254 putative bioactive compound as GA_{Mp}.
255

256 **MpKOL1 and MpKAOL1 catalyze the biosynthesis of KA and GA_{12}, respectively**

257 The enzymatic activities for MpCPS to produce *ent*-copalyl diphosphate and MpKS
258 (Mp6g05950) to produce *ent*-kaurene have been biochemically confirmed in the previous
259 research (Kumar et al., 2016). To find the downstream enzymes catalyzing KA and GA_{12}
260 biosynthesis in *M. polymorpha*, we tested the enzymatic activity of KO and KAO homologs
261 (Figure 4A). Three KO homologs were identified by phylogenetic analysis in *M. polymorpha*
262 (Supplemental Figure 8), and each of them was expressed in the methylotrophic yeast *Pichia*
263 *pastoris* together with the *Arabidopsis* CYTOCHROME P450 REDUCTASE 1 (AtCPR1,
264 AT4G24520). The yeasts were co-cultured with the substrate (*ent*-kaurene) for two days, then
265 the culture infiltrates were extracted and analyzed with gas chromatography-mass spectrometry
266 (GC-MS). KA was generated as a major product in the yeast culture expressing MpKOL1
267 (Mp3g18320), but not detected in cultures expressing MpKOL2 (Mp2g01950) or MpKOL3
268 (Mp2g01940) (Figure 4B; Supplemental Figure 6B).
269 All currently known plant-type KAOs belong to the CYP88 family, in which two *M. polymorpha*
270 members (MpKAOL1, Mp4g23680; and MpKAOL3, Mp2g10420) were confirmed by our
271 phylogenetic analysis. Previous analysis considered the protein encoded by Mp1g25410 as a
272 KAO homolog and named it MpKAOL2 (Bowman et al., 2017). In our current analysis, this
273 protein and its liverwort homologs were closely related to CYP729 family members, which are
274 distinctively different from CYP88 proteins (Supplemental Figures 9-10). After two day's culturing,

275 *Pichia* cells expressing MpKAOL1 showed a clear consumption of KA and production of GA_{12},
276 which displayed identical retention time and mass spectra with the major product from the
277 AtKAO1-expressing culture, i.e. the positive control. While in the MpKAOL3-expressing culture,
278 consumption of KA was limited and no GA_{12} production was detected (Figure 4C-D,
279 Supplemental Figure 6B). It seems that MpKOL1 and MpKAOL1, but not their *M. polymorpha*
280 homologs, harbor catalytic activities similar to angiosperm GA biosynthesis enzymes.

281 By expressing Citrine-fused proteins under the control of the 35S promoter, we observed the
282 subcellular localization of the four *M. polymorpha* enzymes which showed catalytic activities
283 related to GA biosynthesis (Supplemental Figure 11). MpCPS-Cit and MpKS-Cit proteins were
284 localized in the chloroplasts, most likely in the stroma as the Citrine signal intensities displayed
285 complementary patterns to the thylakoid-enriched chlorophyll (Supplemental Figure 11A-B). The
286 signals of MpKOL1-Cit proteins were also associated with chloroplasts, being strongest in
287 chloroplast envelopes (Supplemental Figure 11C). On the other hand, MpKAOL1-Cit proteins
288 seemed to aggregate in the endomembrane system and could be observed near the nuclear
289 envelope and the plasma membrane (Supplemental Figure 11D). Overall, the subcellular
290 distribution of these proteins were similar to their homologs in *A. thaliana* (Sun and Kamiya,
291 1994; Helliwell et al., 2001b), supporting them as being evolutionary conserved in land plants.

292

293 **KA is a pivotal intermediate in the biosynthesis of GA-related hormone**

294 To validate the physiological role of GA biosynthesis enzymes other than MpCPS *in vivo*, we
295 created loss-of-function mutants for all KS, KO and KAO homologs in *M. polymorpha*, using the
296 CRISPR/Cas9^{D10A} nickase or the CRISPR/Cas9 system (Supplemental Figure 2B-D;
297 Supplemental Figure 12). Consistent with the enzymatic activities in yeast or *in vitro* (Kumar et
298 al., 2016), Mp*ks-14*^{ld}, Mp*kol1-7*^{ld}, and Mp*kaol1-7*^{ge} mutants completely lost the ability to produce
299 GA_{12} endogenously (Figure 4E; Supplemental Figure 6C-D). Under cW+cFR conditions, the
300 phenotypes of Mp*ks*^{ld} and Mp*kol1*^{ld} mutants were similar to that of Mp*cps*^{ld}. The thalli of these
301 mutants were significantly larger, wider and flatter than those of wild-type plants (Figure 4F-G).
302 Mp*ks*^{ld} and Mp*kol1*^{ld} mutants were delayed in gametangiophore formation, and their
303 antheridiophores had fan-shaped receptacles and short thick stalks (Figure 4H-I). As MpKS and
304 MpKOL1 catalyze reactions prior to KA biosynthesis, we tested if KA could rescue the
305 phenotypes of Mp*ks*^{ld} and Mp*kol1*^{ld}. Indeed, 2-μM KA application fully restored the thallus

306 morphology and gametangiophore formation in these mutants, which further supported that KA
307 biosynthesis has a pivotal role in the FR response of *M. polymorpha* (Figure 4F-I).
308 In addition to MpKS, the other TPS-e/f clade member, MpTPS1 (Mp6g05430), is known to
309 produce *ent*-kaurene as a minor product (Kumar et al., 2016). However, Mp*tps1*^{ld} mutants
310 showed similar morphology to wild-type plants under cW or cW+cFR conditions, suggesting that
311 Mp*TPS1* is not a major gene required for GA_{Mp} biosynthesis (Supplemental Figure 12A;
312 Supplemental Figure 13). Mp*KOL2* and Mp*KOL3*, the homologs of Mp*KOL1*, are tandemly
313 arranged in the genome, so we removed the whole genomic fragment containing both genes
314 with CRISPR/Cas9^{D10A} nickase (Supplemental Figure 12B). Again, no phenotype related to FR
315 response was observed, which is consistent with the lack of KA-producing activity for both
316 enzymes (Supplemental Figure 13).
317 As MpKAOL1 could catalyze the KA to GA_{12} conversion, we hypothesized that this is a
318 reaction leading to the biosynthesis of GA_{Mp} in *M. polymorpha*. As a fact, Mp*kaol1*^{ge} mutants
319 were defective in FR response, in a manner similar to the KA biosynthesis mutants. After 12
320 days of growth under cW+cFR, large wide and flat thallus was observed in Mp*kaol1*^{ge} mutants
321 (Figure 4F-G). Since MpKAOL1 is likely to act downstream of KA synthesis, these mutants were
322 not supposed to be very sensitive to KA treatment. In the experiments, although 2 μM of KA
323 slightly altered the thallus morphology under cW+cFR, while no significant changes could be
324 observed at concentrations equal to or lower than 1 μM (Figure 4F-G; Supplemental Figure 7B-
325 E). Mp*kaol1*^{ge} mutants also showed a moderate delay in gametangiophore formation, which was
326 insensitive to KA treatment. However, the antheridiophore morphology of Mp*kaol1*^{ge} mutants
327 was similar to that of wild-type plants, suggesting that the biosynthesis of GA_{Mp} might not be
328 completely abolished by Mp*kaol1*^{ge} (Figure 4H-I). Complete deletion of the other KAO homolog,
329 Mp*kaol3*^{ld}, failed to show any severe defects in FR response, yet double mutants would be
330 needed for future research to carefully examine the redundancy with MpKAOL1 (Supplemental
331 Figures 12C and 13).
332
333 **FR enrichment induced GA biosynthesis in a Mp*PIF*-dependent manner**
334 Recent research reported that several GA biosynthesis genes were up-regulated under FR-
335 enriched light conditions (Briginshaw et al., 2022). In our previous transcriptome data
336 (Hernández-García et al., 2021), irradiation solely with FR light significantly increased the

337 expression of Mp*KOL1* within 1 h, and the expression of Mp*CPS* and Mp*KAOL1* after 4 h of
338 treatment. Such responses were only seen in the wild-type plants but not the Mp*pif*^{ko} mutant,
339 indicating that it is a process controlled by the Mpphy-MpPIF signaling module (Supplemental
340 Figure 14A). Similarly, when we transferred 7-day-old plants grown under cW conditions to
341 cW+cFR, Mp*PIF*-dependent up-regulation of Mp*CPS*, Mp*KS*, Mp*KOL1* and Mp*KAOL1*
342 expression could be detected by quantitative polymerase chain reaction (qPCR) within 24 h
343 (Figure 5A, Supplemental Figure 14B). Interestingly, Mp*KOL1* showed a slightly different
344 expression pattern to the other three genes. MpKOL1 expression peaked at 8 h after induction
345 but slightly decreased at the 24-h time point, while the expression of Mp*CPS*, Mp*KS* and
346 Mp*KAOL1* gradually increased in the 24 h after induction, which might reflect different modes of
347 transcriptional regulation. Consistent with the gene expression, we detected a higher level of
348 endogenous GA_{12} in plants induced with cW+cFR than those kept under cW conditions, which
349 suggested the accumulation of GA-related compounds under FR-enriched conditions (Figure
350 5B).
351

352 **GA-related hormone regulated transcriptional responses to FR enrichment**

353 To explore gene expression changes related to GA biosynthesis in *M. polymorpha*, we
354 analyzed transcriptomes from thalli grown under cW or cW+cFR for 12 days, either of wild-type
355 plants, or of Mp*cps-4*^{ld} mutants with or without 2-μM KA treatment. In agreement with the mild
356 change in thallus morphology, only a few genes were differentially expressed between Mp*cps-*
357 *4*^{ld} and wild-type plants under cW conditions (Figure 5C; Supplemental Data Set 1). In particular,
358 the expression of Mp*TPS6*, which encodes an enzyme producing *cis*-kolavenol (Jia et al., 2022),
359 was significantly decreased in Mp*cps-4*^{ld} and rescued by KA under cW. In contrast, 780 and 257
360 genes were down- and up-regulated, respectively, in Mp*cps-4*^{ld} mutants under cW+cFR,
361 suggesting a more active function of GA_{Mp} under FR-enriched conditions. A proportion of the
362 differentially expressed genes could be rescued by KA application (Figure 5C; Supplemental
363 Data Set 1). For most of the Mp*cps*^{ld}-affected genes, the expression was strongly altered by FR
364 enrichment in the wild-type plant, and the differential expression in Mp*cps-4*^{ld} was essentially
365 the reduction in FR-induced gene expression change (Figure 5D). If we compare the
366 transcriptomes between cW+cFR and cW, the numbers of up- and down-regulated genes both
367 declined by more than 60% in the Mp*cps-4*^{ld} mutant (Figure 5E).

368 Using fussy gene ontology (GO) annotations generated with the Blast2GO algorithm (Conesa
369 and Götz, 2008; Hernández-García et al., 2021), we performed GO enrichment analyses for
370 biological processes on differentially expressed genes in Mp*cps-4*^{ld} under cW+cFR (Figure 5F;
371 Supplemental Data Set 2). Although KA application rescued only a limited proportion of gene
372 expression changes in Mp*cps*^{ld}, the patterns of enriched GO terms were quite similar in both
373 comparisons. Mp*cps-4*^{ld} down-regulated or KA-upregulated genes were enriched in GO terms
374 related to stress response and secondary metabolism, among which top-ranked the
375 phenylpropanoid metabolic process. When we carefully checked gene homologs, 23 genes
376 putatively catalyzing biosynthesis of auronidins, bibenzyls or lignin monomers were up-regulated
377 by FR enrichment in a Mp*CPS*-dependent manner (Supplemental Figure 15A). In the Mp*cps-4*^{ld}
378 down-regulated gene set, we also found 30 CYPs, 12 2-OGDs and 7 uridine 5'-diphospho-
379 glucuronosyltransferases (UGTs), all of which were mostly homologs specific to *M. polymorpha*
380 or liverworts, possibly associated with lineage-specific metabolites (Supplemental Figure 15B-
381 D). It seemed that *M. polymorpha* was allocating more resources to stress and defense
382 responses under FR-enriched conditions, yet less doing so when GA_{Mp} biosynthesis was
383 defective. On the other side, GO enrichment captured photosynthetic genes in the Mp*cps-4*^{ld} up-
384 regulated gene set (Figure 5F), which suggested that this mutant might be more resistant to FR-
385 induced chlorophyll reduction (Fredericq and de Greef, 1966). Cell-wall related enzymes and
386 peroxidases were found in both down- and up-regulated gene sets, which was in agreement with
387 the change in thallus growth allometry caused by FR enrichment or Mp*cps*^{ld}, but might also be
388 related to stress and defense responses (Supplemental Figure 15E-F).
389 Gene expressions of several phytohormone pathways were altered by Mp*cps*^{ld} under cW+cFR.
390 First of all, FR-induction of Mp*KS* and Mp*KAOL1* was reduced in Mp*cps-4*^{ld}, which suggested
391 that GA biosynthesis might be regulated by positive feedback in *M. polymorpha* (Supplemental
392 Figure 15G). Such an effect was confirmed with qPCR, in which 3 days of KA treatment partially
393 restored Mp*KS* and Mp*KAOL1* expression (Figure 5G). Mp*KOL1* expression was not affected
394 by Mp*cps*^{ld} or KA treatment, suggesting that it is not a target for such feedback regulation. For
395 cytokinin, the biosynthesis enzymes Mp*IPT2* and Mp*LOG*, and the deactivation enzyme
396 Mp*CKX2* were down-regulated in Mp*cps-4*^{ld} (Supplemental Figure 15G). Previous research
397 showed that Mp*CKX2* overexpression reduced the level of cytokinins, restricted thallus growth
398 and increased thallus hyponasty under cW (Aki et al., 2019). It is possible that FR enrichment

399 changed the thallus growth via coordinated deactivation of cytokinins and accumulation of GA_{Mp}.
400 Furthermore, expression of three abscisic acid (ABA) metabolic genes (MpABA4, MpNCED,
401 MpCYP707A) and more than 40 ABA-responsive, LATE EMBRYOGENESIS ABUNDANT-like
402 (LEA-like) proteins were induced by FR enrichment, similar to the response in *A. thaliana*
403 (Michaud et al., 2023) (Supplemental Figure 15H). Such induction was reduced in Mp*cps-4*^{ld} and
404 restored by KA application, which showed similar tendency as the overall stress response.
405

406 **DISCUSSION**

407 Light quality, i.e. the ratio of red and far-red lights, is an important environmental clue for nearly
408 all land plants to optimize their growth and photosynthesis efficiency. Using a reverse-genetic
409 approach, we showed that biosynthesis of gibberellin-related diterpenoids is required for many
410 aspects of FR response in the liverwort *M. polymorpha*. Under FR-enriched conditions, wild-type
411 plants often develop narrow and hyponastic thallus and begin to form gametangiophores, which
412 is accompanied with increased expression of GA biosynthesis genes and accumulation of GA_{12}
413 (Figures 1, 2, 5) (Fredericq and de Greef, 1966; Briginshaw et al., 2022). In contrast, Mp*cps*^{ld}
414 and other GA biosynthesis mutants developed wide and flat thallus, with a delay in the
415 gametangiophore formation (Figures 1, 2, 4). Application of the biosynthesis intermediate KA
416 rescued all mutants deficient of its biosynthesis (Figures 3, 4), indicating that these phenotypes
417 were likely caused by the deficiency of some KA-derived diterpenoid compound(s), which we
418 named GA_{Mp}. In angiosperms, GA constantly modulates growth and development throughout
419 the life cycle, mostly by promoting growth via cell elongation and/or cell division (Hedden, 2020).
420 But in *M. polymorpha*, GA_{Mp} deficiency had little influence on the vegetative growth under white
421 light conditions. The bioactivity of GA_{Mp} was observed only after its induced accumulation under
422 FR-enriched conditions, suggesting that it served as a hormone coping with environmental
423 changes, rather than constitutively regulating growth. Moreover, the thallus size was increased
424 in GA_{Mp} biosynthesis mutants under cW+cFR (Figures 1, 4), implying that GA_{Mp} actively inhibits
425 rather than promotes growth in the gametophyte of *M. polymorpha*.

426 FR enrichment induced hyponastic growth in the thallus of *M. polymorpha*, which is
427 comparable to the increase of leaf hyponasty in shade-avoiding angiosperms. In *A. thaliana*, FR
428 enrichment triggers the hyponastic growth by preferentially enhancing cell elongation in the
429 abaxial side of the petiole (Küpers et al., 2023). While in *M. polymorpha*, such response relies

430 on the regional growth driven by apical meristems. In previously reported end-of-day FR
431 irradiation experiments, if the treatment was discontinued after several cycles, the newly-grown
432 apical region resumed pleiotropic orientation, while the basal part remained hyponastic
433 (Fredericq and Greef, 1968). With EdU analysis, we observed cell division patterns under FR-
434 enriched conditions, which was most active near the apical meristem. The hyponastic growth in
435 wild-type plants were marked with excessive cell division in the ventral side of the thallus,
436 implying a role for differential cell proliferation in this process. The large and flat thallus of Mp*cps*^{ld}
437 mutants have more actively dividing cells in total, which showed no dorsiventrally biased
438 distribution (Figure 1). Since Mp*cps*^{ld} phenotypes could be complemented by expression of
439 Mp*CPS* using the constitutive 35S promoter, which was equally active in dorsal and ventral
440 tissues (Althoff et al., 2014), it is unlikely that FR-induced hyponasty is established directly by
441 differential biosynthesis of GA_{Mp}. This is similar to the situation in *A. thaliana* petioles, where GA
442 served as a modulator for FR-induced hyponasty but showed no biased adaxial-abaxial activity
443 (Küpers et al., 2023).

444 The erected, stalked gametangiophores of *M. polymorpha* could be considered as an extreme
445 form of hyponastic growth, and dorsal tissues were evidently reduced in the cylindrical stalks of
446 wild-type plants (Shimamura, 2016). The stalks of Mp*cps*^{ld} gametangiophores were relatively
447 short and thick, bearing dorsal air chambers similar to the vegetative thallus, which showed less
448 biased dorsoventral growth (Figure 2; Supplemental Figure 5). This phenotype resembled that
449 of Mp*kanadi* (Mp*kan*), which was depleted of the sole *M. polymorpha* homolog for KANADI, a
450 family of transcription factors regulating tissue polarity in angiosperms (Briginshaw et al., 2022).
451 Under cW+cFR, both Mp*kan* and Mp*cps*^{ld} mutants were reduced in hyponasty, formed thallus-
452 like gametangiophores with delay but generated fertile gametes, which could be explained by
453 the dysfunction of Mp*kan* to up-regulate the expression of GA_{Mp} biosynthesis genes in response
454 to FR irradiation (Briginshaw et al., 2022).

455 By tracing germ cell progenitors with MpBNB accumulation, we found that Mp*cps*^{ld} mutants
456 were delayed in germline differentiation (Figure 2). Many fern species use GA-related
457 pheromones, i.e. antheridiogens, to control germline differentiation in the population. Particularly,
458 antheridiogens promote the formation of male antheridia, and inhibits female archegonia in
459 undifferentiated gametophytes (Näf et al., 1975; Tanaka et al., 2014; Hornych et al., 2021). In
460 *M. polymorpha*, sexual differentiation is known to be determined by a sex chromosome-located

461 gene (Iwasaki et al., 2021), and MpBNB accumulation was similarly delayed in both male and
462 female Mp*cps*^{ld} gametophytes, suggesting no sexual bias in the function of GA_{Mp}.
463 We partially elucidated the biosynthetic pathway of GA_{Mp} with biochemical and genetic
464 approaches. Previous bioinformatic research suggested that early steps of GA biosynthesis are
465 conserved in land plants, and the *M. polymorpha* genome contains multiple homologs for KO
466 and KAO (Bowman et al., 2017; Cannell et al., 2020; Yoshida et al., 2020). Using the yeast
467 expression system, we detected the production of KA by MpKOL1 and GA_{12} by MpKAOL1,
468 showing the two enzymes possessing enzymatic activities similar to their angiosperm homologs.
469 Genetic analyses also supported that KA is synthesized via the sequential action of three single
470 enzymes (Mp*CPS*, Mp*KS*, and Mp*KOL1*), as their mutants were consistently defective in FR
471 light responses (Figure 4). Intriguingly, although GA_{12} production was almost completely blocked
472 in Mp*kaol1*^{ge} mutants, we only saw morphological phenotypes in the vegetative thallus, but not
473 in the gametangiophores. As monooxygenases, it takes three sequential steps for CYP enzymes
474 to catalyze the KA-to-GA_{12} conversion, first from KA to *ent*-7-hydroxy-kaurenoic acid (7OH-KA),
475 then from 7OH-KA to GA_{12}-aldehyde, and finally from GA_{12}-aldehyde to GA_{12} (Helliwell et al.,
476 2001a). In the GA-producing fungus *Fusarium fujikuroi*, even though GA_{12} production still occurs,
477 it is largely bypassed through 3β-hydroxylation of GA_{12}-aldehyde to form GA_{14}-aldehyde, which
478 is then converted into GA_{14} and other gibberellin compounds (Hedden et al., 1974; Urrutia et al.,
479 2001; Rojas et al., 2001). Therefore, we could not conclude that Mp*kaol1*^{ge} mutant phenotypes
480 were caused by deficiency in GA_{12} production, and MpKAOL1 might work redundantly with other
481 enzymes to produce other intermediates, synthesizing GA_{Mp} in a GA_{12}-independent pathway.
482 Despite the conserved activities of MpKOL1 and MpKAOL1, we detected no KA synthesis
483 activity for MpKOL2 or MpKOL3, and no GA_{12} production by MpKAOL3 (Figure 4). Also, no
484 morphological abnormality related to far-red light response was observed in their loss-of-function
485 mutants, suggesting that they are not major enzymes required for GA_{Mp} biosynthesis
486 (Supplemental Figure 13). In the phylogenetic tree of KOs (CYP701s) (Supplemental Figure 8),
487 all liverwort homologs formed a monophyletic clade with two major subclades, both containing
488 sequences from Jungermanniopsida and Marchantiopsida species. MpKOL2 and MpKOL3
489 belong to a subclade different from MpKOL1, suggesting these KO homologs were diverged
490 soon after the emergence of the most recent liverwort common ancestor. The phylogenetic
491 relationship of KAOs (CYP88s) from liverworts and hornworts is less clear, but similarly,

492 MpKAOL1 and MpKAOL3 belong to different clades deeply diverged in liverworts (Supplemental
493 Figure 9). It remains to be explored if such divergence contributes to the diversification of
494 diterpenoid metabolism in liverworts.

495 Comparing the biosynthesis of GA-related diterpenoids between *M. polymorpha* and *P. patens*,
496 we see both conservation and divergence of this pathway in evolution. On the one hand, both
497 bryophyte species share the biosynthesis route for KA with vascular plants. KO is present in
498 almost all genomes and transcriptomes included in our phylogenetic analysis. As a recent study
499 proposed that the ancestral *TPS* gene in land plants encoded a bifunctional CPS/KS enzyme
500 (Jia et al., 2022), it is possible that production of KA is conserved in all major lineages of land
501 plants. On the other hand, *M. polymorpha* and *P. patens* seem to take different routes to
502 synthesize bioactive compounds from KA. Consistent with the lack of KAO (CYP88) homologs
503 in all mosses, *P. patens* produced *ent*-3β-hydroxy-kaurenoic acid (3OH-KA) and *ent*-2α-hydroxy-
504 kaurenoic acid (2OH-KA) from KA, with the former having physiological activities on protonemal
505 cell differentiation (Miyazaki et al., 2018). Meanwhile, the production of GA_{12} in *M. polymorpha*
506 opened the possibility of using C20-GAs in growth regulation, although no common GA from
507 angiosperms was detected in either bryophyte species (Figure 3) (Hayashi et al., 2010).

508 Due to the lack of GIBBERELLIN-INSENSITIVE DWARF1 (GID1) receptors in bryophytes, it
509 is unlikely that GA-related hormones are perceived by the canonical GID1-DELLA module in *M.*
510 *polymorpha* or *P. patens*. Previously we reported that overexpression of Mp*DELLA* inhibited
511 MpPIF-mediated FR responses, reducing gemma dormancy and delaying the formation of
512 gametangiophores (Hernández-García et al., 2021). However, Mp*DELLA* overexpression
513 strongly inhibited cell division and thallus growth, which was opposite to the effect of GA_{Mp}
514 deficiency. It is possible that the functions of GA_{Mp} and MpDELLA remain uncoupled in *M.*
515 *polymorpha*.

516 Gene expression analysis confirmed that Mp*CPS*, Mp*KS*, Mp*KOL1* and Mp*KAOL1* were
517 induced by FR enrichment in an Mp*PIF*-dependent manner (Figure 5). The regulatory role of
518 Mp*PIF* is further supported by phenotypic similarities between GA_{Mp} biosynthesis mutants and
519 Mp*pif*. Under FR enriched conditions, Mp*pif* mutants developed wider, flatter and larger thallus,
520 and failed to form any gametangiophores (Inoue et al., 2019; Streubel et al., 2023). In
521 angiosperms, FR enrichment also activates the expression GA biosynthesis enzymes, yet more
522 frequently regulating 2-OGD family genes such as GA20ox or GA3ox (Hisamatsu et al., 2005;

523 Kohnen et al., 2016; Küpers et al., 2023), which are absent from bryophytes. Considering the
524 putatively different mechanism for GA perception, GA biosynthesis might be independently
525 incorporated into the gene regulatory network by liverworts and angiosperms in evolution, in
526 response to the common threat of a FR-enriched environment.
527

528 **METHODS**

529 **Plant materials and maintenance**

530 The *M. polymorpha* subsp. *ruderalis* accessions Takaragaike-1 (Tak-1) and Takaragaike-2
531 (Tak-2) were used as male and female wild-type materials, respectively (Ishizaki et al., 2008).
532 For maintenance, *M. polymorpha* plants were cultured aseptically on half-strength Gamborg's
533 B5 medium (Gamborg et al., 1968) with 1% agar at 22°C under continuous white light (40-50
534 μmol photons m^{-2} s^{-1}), which was supplemented by cold cathode fluorescent lamps (CCFLs,
535 OPT-40C-N-L from Optrom, Japan). If not specified, this medium and temperature was used for
536 all aseptic cultures for *M. polymorpha*.
537

538 **Light sources**

539 In all the experiments, plants were cultured under continuous white light conditions (cW,
540 approximately 40 μmol photons m^{-2} s^{-1}) with or without continuous far-red light (cFR,
541 approximately 25 μmol photons m^{-2} s^{-1}). For thallus morphology observation, cW and cFR were
542 supplemented by CCFLs and light-emitting diodes (LEDs), respectively, in the multi-chambered
543 incubator (LH-80CCFL-6CT from NK systems, Japan). For gametangiophore induction of
544 aseptic cultures, cW was supplemented by CCFLs (ST-40C-BN, Shinshu Trading, Japan) and
545 cFR was supplemented by LEDs (IR LED STICK, NAMOTO, Japan). For plants grown on the
546 vermiculite, cW was supplemented by fluorescent tubes (FLR40SN/M/36, Toshiba, Japan) and
547 cFR was supplemented by LEDs (VBL-TFL600-IR730, Valore, Japan).
548

549 **Construction of mutants and transgenic plants**

550 To create large-deletion mutants of a target gene, four guide RNAs (gRNAs) with target
551 sequences flanking the CDS were first cloned separately into pMpGE_En04, pBCGE12,
552 pBCGE23 and pBCGE34 (Hisanaga et al., 2019; Koide et al., 2020) by ligation of BsaI-digested
553 vectors with annealed complementary DNA oligos. Then the fragments containing the MpU6-1

554 promoter and gRNAs were digested from the pBCGE12, pBCGE23 and pBCGE34 constructs
555 and inserted between the BglI sites of the pMpGE_En04 construct to create a multiplex entry
556 vector. Finally, this entry vector was recombined with pMpGE017 or pMpGE018 (Hisanaga et
557 al., 2019) using Gateway LR Clonase II (Thermo Fisher Scientific) to generate the binary vector
558 for plant transformation. To generate the Mp*kaol1*^{ge} mutants, the gRNA was designed to target
559 sequences near the start codon of Mp*KAOL1*. The corresponding DNA oligos were annealed
560 and ligated into the BsaI sites of pMpGE_En03, then subcloned to the binary vector pMpGE011
561 (Sugano et al., 2018).

562 For the complementation of mutants and/or subcellular localization observations, CDSs of
563 Mp*CPS*, Mp*KS*, Mp*KOL1* and Mp*KAOL1* were amplified from the complementary DNA (cDNA)
564 of Tak-1 plants and directionally cloned into pENTR/D-TOPO (Thermo Fisher Scientific) to
565 create entry vectors without stop codon. To mutate the gRNA target sequence in Mp*KAOL1*, the
566 whole plasmid of pENTR-MpKAOL1-CDS was amplified with the site-directed mutagenesis
567 primers MpKAOL1-mut-F and MpKAOL1-mut-R, then re-circularized to generate pENTR-
568 MpKAOL1-CDSmut. All the CDSs were then subcloned from entry vectors to pMpGWB106 or
569 pMpGWB306 using Gateway LR reactions, which were used for expressing the target proteins
570 under the 35S promoter with an in-frame Citrine fusion at the C terminus (Ishizaki et al., 2015).

571 All the binary vectors were introduced into *M. polymorpha* by transformation of regenerating
572 thalli using the *Agrobacterium tumefaciens* strain GV2260 as previously described (Kubota et
573 al., 2013). Successful mutations were identified by genotyping PCR and Sanger-sequenced to
574 confirm non-identical alleles. See Supplemental Tables 1-3 for full lists of plant materials
575 generated by this research, and the plasmids and DNA oligos used for construction.

576

577 **Measurement of thallus morphology**

578 For thallus morphological observation, plants were grown from gemmae on the medium
579 containing 1% sucrose under cW or cW+cFR in a multi-chambered incubator (LH-80CCFL-6CT
580 from NK systems, Japan). After 12 days of growth, camera photos of the plants were taken
581 vertically from the top. Then medium blocks with individual plants were carefully cut out, aligned
582 at a certain distance to a fixed camera for taking side-view photos. Typically, the two apical
583 meristems from one gemma both develop into mature thallus branches, and we define the part
584 developed from a single gemma meristem as a “half thallus”. These half thalli were cut apart,

585 flattened on a filter paper and photographed for the measurements of length, width and area. All
586 the measurements were done in Fiji (Schindelin et al., 2012) as describe in Supplemental Figure
587 16 with in-house macro scripts, which are available at
588 https://github.com/dorrenasun/Mp_GA_biosynthesis. Data was excluded for a whole plant if
589 more than two apical meristems were active in the gemma, or for a half thallus if it showed severe
590 defects in dorsoventral differentiation.
591

592 **EdU assay**

593 To analyze the cell division activity, plants were grown on the medium containing 1% sucrose
594 under cW+cFR for 7 days, then soaked for 2 h in liquid half-strength Gamborg's B5 medium
595 containing 20 mM 5-ethynyl-2'-deoxyuridine (EdU). Then the samples were fixed in 3.7%
596 formaldehyde for 1 h, washed twice with phosphate buffer saline (PBS, 5 min each), and treated
597 with 0.5% Triton X-100 in PBS for 20 min. After two washes with 3% bovine serum albumin
598 (BSA) in PBS, the samples were kept in the reaction mixture from the Click-iT EdU Imaging Kit
599 with Alexa Fluor 555 (Thermo Fisher Scientific, #C10338) for 1 h in darkness, then washed twice
600 with PBS before soaked overnight in 20% caprylyl sulfobetaine (#D4246, TCI, Japan) to remove
601 the chlorophyll. After another two washes with PBS, the thalli were treated with 75.5% (w/v)
602 iohexol (GE Healthcare Pharma) for 1 h and mounted on glass slides following the iTOMEI
603 protocol (Sakamoto et al., 2022). Image stacks of the apical regions were obtained with a
604 confocal laser scanning microscope (Olympus FLUOVIEW FV1000) at 5-μm steps in the z
605 direction. Excitation and emission wavelengths were 543 nm and 505-605 nm, respectively.
606 Numbers of EdU-positive nuclei were quantified in the Z-projections of the image stacks using
607 the StarDist plugin of Fiji and in-house scripts (Schmidt et al., 2018; Schindelin et al., 2012).
608

609 **Observation of gametangiophores**

610 To observe the progress of gametangiophore formation in aseptic culture, plants were first
611 grown from gemmae on the medium containing 1% sucrose under cW for 7 days, then half thalli
612 developed from single gemma meristems were cut apart and cultured on fresh medium plates
613 under cW+cFR. Chemical treatments were included in the medium of second-stage culturing,
614 starting together with the FR irradiation. Apical regions of each plant were observed under a
615 stereoscope (Olympus SZX16) every day, and the emergence of gametangiophores was

616 recorded if a stalk or dark-green primordia was formed. Images of gametangiophores were taken
617 with stereoscopes (Olympus SZX16 or Leica M205C). For morphological observation of
618 gametangiophores, the plants were also grown on the vermiculite in the open air. After an initial
619 culturing of 7-14 days from gemmae under aseptic maintenance conditions, thallus fragments
620 were planted in pots containing vermiculite and grown under cW+cFR conditions with regular
621 watering. For sectioning of gametangiophores, fresh stalks or receptacles were embedded in 5-
622 6% agar and sectioned with a vibratome (DOSAKA LinearSlicer Pro7) at the desired thickness.
623 Images of the sections were obtained with the microscope under bright field (Keyence BZ-X710).
624

625 **Microscopy of MpBNB-Cit**

626 To capture the early stage of gametangium differentiation, male and female plants carrying
627 the Mp*BNB-Cit* knock-in locus were cultured from gemmae on the medium containing 1%
628 sucrose under cW+cFR for 11 and 14 days, respectively. For male plants, half thalli developed
629 from single gemma meristems were collected for observation. For female plants, the second
630 bifurcation has already occurred, so one of the four apical regions was selected randomly on
631 each plant for observation. Thallus fragments were fixed with 4% paraformaldehyde (PFA) for 1
632 h at room temperature, washed twice with PBS and soaked in the ClearSeeAlpha solution
633 (Kurihara et al., 2021) for 2 days to remove chlorophyll. After that, the samples were washed
634 twice with PBS, stained with 1 mg/mL calcofluor white for 10 min and washed again twice with
635 PBS. Finally, the samples were infiltrated with 75.5% (w/v) iohexol (GE Healthcare Pharma) for
636 1 h and mounted onto slides. Image stacks were obtained with the fluorescent microscope
637 (Keyence BZ-X710) at 5-μm steps and processed into full-focus projections with BZ-X Analyzer,
638 and the number of Citrine-positive nuclei was counted in Fiji (Schindelin et al., 2012). The BZ-X
639 DAPI (Excitation: 360±20 nm; Emission: 460±25 nm; Dichroic mirror: 400 nm) and customized
640 (Excitation: 500±10 nm; Emission: 535±15 nm; Dichroic mirror: 515 nm) filters were used for
641 acquiring signals from calcofluor white and Citrine, respectively.
642

643 **LC-MS/MS analysis of endogenous GAs**

644 To analyze the endogenous GAs, most plants were cultured from gemmae on the medium
645 containing 1% sucrose under cW for 10 days, then under cW+cFR for another 4 days. Tak-1
646 wild-type plants were also cultured under cW for 14 days to examine the effect of FR enrichment.

647 For each sample, 3 g of thallus tissue was harvested, frozen with liquid nitrogen, and stored at -
648 80 °C before extraction. To prepare samples for LC-MS/MS analysis, each frozen sample was
649 homogenized in 15 mL acetone with $^{2}H_{2}$-labelled authentic compounds, then left at 4 °C for a 2-
650 h extraction. After filtering with defatted cotton, the acetone extract was concentrated to
651 approximately 1 mL with nitrogen blow and mixed with 1 mL acetonitrile. The mixture was
652 extracted for 3 times with 2 mL hexane, and the remaining aqueous phase was alkalified with 1
653 mL saturated solution of $NaHCO_3$. After two more extractions with 2 mL chloroform, the aqueous
654 phase was passed through a cartridge filled with polyvinylpyrrolidone (PVP), acidified to pH2-3
655 with HCl (6 M), and sequentially purified with a reverse-phase cartridge (Oasis HLB 3 cc/60 mg,
656 Waters), an anion-exchange cartridge (Bond Elut DEA 100 mg/1 mL, Agilent), and a silica
657 cartridge (Sep-Pak Silica 1 cc Vac Cartridge, Waters). The final elute was dried up with a vacuum
658 centrifuge concentrator and dissolved in 1% acetic acid before loading to the LC-MS/MS.
659 The LC-MS/MS system consisted of an ultra-performance LC (ExionLC, Sciex) equipped with
660 a reverse-phase column (CORTECS UPLC C18+, φ1.6 μm, 2.1×100 mm, Waters) and a
661 quadrupole time-of-flight mass spectrometer (X500R QTOF, Sciex). LC separations were
662 performed at 40 °C with a flow rate of 0.3 mL/min using solvent A (0.05% acetic acid in water)
663 and solvent B (0.05% acetic acid in acetonitrile) and the following program: a linear gradient of
664 B from 3% to 65% over 17 min, followed by an isocratic elution with 98% of B for 2 min.
665 Quantification of GAs was performed in the multiple reaction monitoring (MRM) mode, and the
666 mass spectrum of GA_{12} was confirmed in the TOF-MS/MS mode.
667
668 **Phylogenetic analysis**
669 For the phylogenetic analysis of KO and KAO homologs, the known protein sequences from
670 *A. thaliana* and *Oryza sativa* were used as the input for BLAST (Altschul et al., 1990) search in
671 the annotated proteins from published genomes and transcriptomes (See Supplemental Data
672 Set 3 for a full list of species and references). Considering the relative low redundancy of these
673 enzymes, the top 20 BLAST hits from each species were retrieved and aligned with MAFFT
674 using the progressive FFT-NS-2 algorithm (Katoh and Standley, 2013). After removing the
675 positions with >80% gaps, an initial maximum likelihood phylogenetic tree was built with all
676 candidate sequences using IQ-TREE 2 with automatic substitution model selection (ModelFinder)
677 and 1000 bootstraps from the ultrafast bootstrap approximation (UFBoot) (Minh et al., 2020;

678 Kalyaanamoorthy et al., 2017; Hoang et al., 2018). Highly-relevant candidate sequences and
679 outgroup sequences were selected from the initial tree and re-aligned with MAFFT using the L-
680 INS-I algorithm (Katoh and Standley, 2013) and trimmed off positions with >98% gaps. The final
681 maximum likelihood tree was inferred using IQ-TREE 2 with automatic substitution model
682 selection (LG+I+G4 for both KOs and KAOs) and 1000 standard non-parametric bootstraps
683 (Minh et al., 2020; Kalyaanamoorthy et al., 2017; Hoang et al., 2018; Guindon et al., 2010). The
684 complete pipeline including scripts, sequence alignments, and the data file for the phylogenetic
685 trees are available at https://github.com/dorrenasun/Mp_GA_biosynthesis. The ggtree R
686 package suite was used for visualization (Yu, 2022; Xu et al., 2022; Yu, 2020b; Yu et al., 2018,
687 2017).
688

689 **Enzymatic assay in *P. pastoris* and GC-MS analysis**

690 To express MpKOLs and MpKAOLs in the yeast *P. pastoris*, the CDSs were amplified from
691 pENTR-CDS entry vectors and inserted into the pPICZA vector (Thermo Fisher Scientific) with
692 homologous recombination using the seamless ligation cloning extract (SLiCE) from *Escherichia*
693 *coli* (Zhang et al., 2012; Motohashi, 2015). The CDSs of At*KO* (AT5G25900) and At*KAO1*
694 (AT1G05160) were amplified from the cDNA of 14-day-old Col-0 seedlings and cloned into
695 pPICZA with the same method. All these plasmids were transformed into a previously described
696 *P. pastoris* X-33 strain carrying the *A. thaliana* cytochrome reductase gene, At*ATR1*
697 (AT4G24520) (Katsumata et al., 2008), following the manufacturer's protocol. The selected
698 transformants were incubated in 2 mL of BMG medium (100 mM potassium phosphate (pH 6.0),
699 1.34% yeast nitrogen base (YNB), 4×10^{-5}% biotin, 1% glycerol) with shaking at 30 °C until they
700 reached an OD_{600} value of 2. Cells were collected by centrifugation and resuspended in 50 mL
701 of MM medium (1.34% YNB, 4×10^{-5}% biotin, 0.5% methanol), and cultured at 30 °C with shaking
702 and addition of methanol every 24 h (final concentration: 0.5% v/v) to maintain protein induction.
703 After 24 h of initial culturing, substrates (7 μg of *ent*-kaurene, or 15 μg of KA) were added into
704 the medium. After another 48 h of incubation, the supernatants were isolated with centrifugation
705 and extracted two times with equal volume of ethyl acetate. The organic phase from the two
706 extractions were combined together, concentrated *in vacuo*, and derivatized with diazomethane
707 in ether solution. After that, the samples were concentrated to approximately 100 μL with
708 nitrogen blow and subjected to GC-MS analysis with a GC (Agilent 6890) equipped with a DB-1

709 capillary column (15 m/0.25 mm/0.25 μm, Agilent J&W) and a mass selective detector (Agilent
710 5975C MSD, ionization energy at 70 eV). The oven temperature was programmed as described
711 previously (Hayashi et al., 2006).
712
713 **Subcellular localization of proteins**
714 To observe the subcellular localizations of MpCPS, MpKOL1 and MpKAOL1, plants were
715 grown from gemmae on the medium containing 1% sucrose under cW+cFR conditions for 7
716 days. The thallus tissues were fixed with 4% PFA at room temperature for 20 min, washed twice
717 with PBS, and stained with 1 mg/mL calcofluor white for 10 min. After another two washes with
718 PBS, the samples were soaked in 75.5% (w/v) iohexol (GE Healthcare Pharma) for 1 h and
719 mounted onto slides. For MpKS, fresh gemmae from gemma cups were mounted in water. For
720 all experiments, complementation lines which used the 35S promoter to express target proteins
721 fused with Citrine in the C-teminus were used for observation, and the parent lines of genetic
722 mutants were used as the negative control.
723 Fluorescent images were acquired using a confocal microscope (Leica TCS SP8X Falcon)
724 equipped with a hybrid detector (HyD). For the observation of MpCPS-Cit and MpKS-Cit,
725 calcofluor white signals were excited with the 405 nm UV laser, and obtained in the xyz mode
726 within the 425-435 nm wavelength region; the Citrine signals were excited with the the pulsed
727 white light laser (WLL) at 488 nm, and obtained at 500-541 nm with time gating (1.8-12 ns for
728 MpCPS-Cit; 1.2-12 ns for MpKS-Cit); the autofluorescence from chlorophyll was excited with the
729 WLL at 592 nm, and obtained at 680-700 nm. For the observation of MpKOL1-Cit and
730 MpKAOL1-Cit, calcofluor white signals were excited with the 405 nm UV laser, and obtained in
731 at 425-475 nm; the Citrine signals were excited with the WLL at 495 nm, and obtained at 500-
732 530 nm with time gating (1.2-6.0 ns); the autofluorescence from chlorophyll was excited with the
733 WLL at 649 nm, and obtained at 655-755 nm.
734
735 **RNA extraction and qPCR**
736 For qPCR experiments, 50-100 mg of whole thallus was collected for each sample, which is
737 frozen with liquid nitrogen and crashed into fine powders with metal beads in a shaking device
738 (Shake Master Auto, BMS-A20TP, Bio Medical Science, Japan). The total RNA was extracted
739 with the TRIzol reagent (Thermo Fisher Scientific) following the manufacturer's protocol. After

740 treatment with RQ1 RNase-Free DNase (Promega), the total RNA was reverse-transcribed
741 using ReverTra Ace (Toyobo Life Science) and the $(dT)_{20}$ oligo. Quantitative real-time PCR
742 reactions with Taq polymerase prepared following (Pluthero, 1993) and SYBR Green I Nucleic
743 Acid Gel Stain (Lonza) was performed in triplicates using the CFX96 real-time PCR detection
744 system (Bio-Rad) with the following program: an initial denaturation for 30 s at 95 °C, then 40
745 cycles of 5 s at 95 °C followed by 30 s at 60 °C. A standard melting curve analysis was performed
746 at the end of the program to validate amplified products. Mp*EF1* (Mp3g23400) was used as the
747 reference gene for quantification, and the relative gene expression levels were calculated
748 following the method in (Hellemans et al., 2008). All primers for target and reference genes were
749 listed in Supplemental Table 3, and the amplification efficiency for each primer pair was
750 measured with serial dilution of mixed cDNA samples.
751
752 **Transcriptome analysis**
753 For transcriptome analysis, plants were cultured from gemmae on the medium with 1%
754 sucrose, either containing 2 μM KA or the solvent control. After 12 days of growth under cW or
755 cW+cFR, ~50 mg whole thallus was collected for each sample, frozen with liquid nitrogen and
756 homogenized with metal beads in a shaking device (Shake Master Auto, BMS-A20TP, Bio
757 Medical Science, Japan). The total RNA was isolated with the RNeasy Plant Mini Kit (QIAGEN),
758 and the RNA quality was confirmed using the Bioanalyzer RNA 6000 pico assay (Agilent). The
759 mRNA was enriched with the NEBNext Poly(A) mRNA Magnetic Isolation Module (New England
760 Biolabs, #E7490). The library was prepared with the NEBNext Ultra II Directional RNA Library
761 Prep Kit for Illumina (New England Biolabs, #E7760) and amplified using NEBNext Multiplex
762 Oligos for Illumina (96 Unique Dual Index Primer Pairs Set 2, New England Biolabs, #E6442).
763 After quality check with the Bioanalyzer High Sensitivity DNA assay (Agilent), the samples were
764 sequenced with the NextSeq 500 system using the NextSeq 500/550 High Output Kit v2.5 for
765 75 cycles (Illumina). Approximately 7.8 million of single-end reads were obtained for each
766 sample, and automatically de-multiplexed by the BaseSpace Sequence Hub (Illumina).
767 The sequence reads were quasi-mapped to the *M. polymorpha* MpTak_v6.1 genome (Iwasaki
768 et al., 2021) and quantified using Salmon (v1.9.0) (Patro et al., 2017), with U-chromosome
769 transcripts excluded from the index. After that, differential gene expression analysis was
770 performed in R (v4.2.2) with the package DESeq2 (v1.38.3) in default settings (Love et al., 2014).

Gene ontology enrichment analyses was performed with the R package topGO (v2.50.0) (Alexa and Rahnenfuhrer, 2022) using annotations previously described (Hernández-García et al., 2021) and the classic Fisher's exact test, and *p*-values were left unadjusted following the package's instructions. To visualize the enriched terms, semantic similarities were calculated using the R package GOSemSim (v2.24.0) (Yu et al., 2010; Yu, 2020a), and used for building a two-dimensional map with the package Rtsne (Krijthe, 2015). The transcriptome data is deposited to the Sequence Read Archive at the DNA Data Bank of Japan (DDBJ) under the Bioproject PRJDB15786. The scripts for data analysis are available at https://github.com/dorrenasun/Mp_GA_biosynthesis.

Supplemental Data

Supplemental Figure 1. Gibberellin (GA) biosynthesis pathway in vascular plants, showing compounds analyzed or used for treatment in this research.

Supplemental Figure 2. Genotype information for Mp*cps*^{ld}, Mp*ks*^{ld}, Mp*kol1*^{ld}, and Mp*kaol1*^{ge} mutants.

Supplemental Figure 3. Thallus morphology of Mp*cps*^{ld} mutants in Tak-2 background under cW+cFR.

Supplemental Figure 4. Morphology of Mp*cps*^{ld} plants during gametangiophore formation in the aseptic culture.

Supplemental Figure 5. Sections of gametangiophores in wild-type and Mp*cps*^{ld} plants, as well as the fertility test.

Supplemental Figure 6. LC-MS/MS and GC-MS profiles for KA and GA_{12} detection.

Supplemental Figure 7. Response of Mp*cps-4*^{ld} and Mp*kaol1-5*^{ge} to different concentrations of KA.

Supplemental Figure 8. Phylogenetic tree of KO homologs in land plants.

Supplemental Figure 9. Phylogenetic tree of KAO and closely-related CYP enzymes in land plants.

Supplemental Figure 10. Heatmap of percentage identity for KAO and closely-related CYP enzymes in land plants.

Supplemental Figure 11. Subcellular localizations of GA biosynthesis enzymes in *M. polymorpha*.

802 **Supplemental Figure 12**. Genotype information for Mp*tps1*^{ld}, [Mp*kol2* Mp*kol3*]^{ld} and
803 Mp*kaol3*^{ld} mutants.
804 **Supplemental Figure 13**. Phenotypes of Mp*tps1*^{ld}, [Mp*kol2* Mp*kol3*]^{ld} and Mp*kaol3*^{ld}
805 mutants.
806 **Supplemental Figure 14**. Up-regulation of GA biosynthesis genes by FR irradiation.
807 **Supplemental Figure 15**. Heatmaps of genes from selected pathways or gene families,
808 showing differential expression in Mp*cps-4*^{ld} under cW+cFR.
809 **Supplemental Figure 16**. Quantification method for thallus morphology.
810 **Supplemental Table 1**. List of plant materials
811 **Supplemental Table 2**. List of plasmids
812 **Supplemental Table 3**. List of DNA oligos
813 **Supplemental Data Set 1**. Differentially expressed genes in the transcriptome analysis
814 **Supplemental Data Set 2**. Enriched gene ontology (GO) terms in the transcriptome
815 analysis
816 **Supplemental Data Set 3**. List of genome and transcriptome sources for phylogenetic
817 analysis
818
819 **Supplemental References**.
820

821 **AKNOWLEDGEMENTS**

822 The authors thank Ryunosuke Kusunoki for plasmid construction and collecting initial
823 experimental data; Wakako Fukuda for data collection during GC-MS analysis; Takefumi Kondo
824 and Yukari Sando for the support on RNA sequencing; Megumi Iwano for the help on confocal
825 microscopy and Chikako Inoue for plant maintenance. This work has been supported by MEXT
826 KAKENHI Grant Number JP19H05675 and JSPS KAKENHI Grant Numbers JP17H07424,
827 JP22H00417 to T.K.; JSPS KAKENHI Grant Numbers JP 24380060, JP15H04492 to M.N. and
828 H.K.; JSPS KAKENHI Grant Number JP16K18693 to S.M.; as well as the International
829 Collaborative Research Program of Institute for Chemical Research, Kyoto University (Grant
830 Numbers 2020-53, 2021-60, 2022-63, 2023-74) to T.K. and S.Yamaguchi.
831

AUTHOR CONTRIBUTIONS

R.S. and M.O. collected and analyzed most of the final data with the help and supervision from K.M., Y.Y., S.Yamaoka., R.N. and T.K.. M.O., S.M., T.I., K.M., M.N. and S.Yamaguchi analyzed endogenous GAs. S.M. and H.K. assayed enzymatic activity. R.K. performed initial experiments that conceptualized the research. H.K., M.N., S.Yamaguchi and T.K. organized the project. R.S., S.Yamaoka., R.N and T.K. wrote the paper with the review and editing from all authors.

REFERENCES

Achard, P., Gusti, A., Cheminant, S., Alioua, M., Dhondt, S., Coppens, F., Beemster, G.T.S., and Genschik, P. (2009). Gibberellin Signaling Controls Cell Proliferation Rate in Arabidopsis. Current Biology 19: 1188–1193.

Aki, S.S., Mikami, T., Naramoto, S., Nishihama, R., Ishizaki, K., Kojima, M., Takebayashi, Y., Sakakibara, H., Kyozuka, J., Kohchi, T., and Umeda, M. (2019). Cytokinin Signaling Is Essential for Organ Formation in Marchantia polymorpha. Plant and Cell Physiology 60: 1842–1854.

Alexa, A. and Rahnenfuhrer, J. (2022). topGO: Enrichment Analysis for Gene Ontology. R package version 2.50.0.

Althoff, F., Kopischke, S., Zobell, O., Ide, K., Ishizaki, K., Kohchi, T., and Zachgo, S. (2014). Comparison of the MpEF1α and CaMV35 promoters for application in Marchantia polymorpha overexpression studies. Transgenic Res 23: 235–244.

Altschul, S.F., Gish, W., Miller, W., Myers, E.W., and Lipman, D.J. (1990). Basic local alignment search tool. Journal of Molecular Biology 215: 403–410.

Beall, F.D., Yeung, E.C., and Pharis, R.P. (1996). Far-red light stimulates internode elongation, cell division, cell elongation, and gibberellin levels in bean. Can. J. Bot. 74: 743–752.

Bou-Torrent, J., Galstyan, A., Gallemí, M., Cifuentes-Esquivel, N., Molina-Contreras, M.J., Salla-Martret, M., Jikumaru, Y., Yamaguchi, S., Kamiya, Y., and Martínez-García, J.F. (2014). Plant proximity perception dynamically modulates hormone levels and sensitivity in Arabidopsis. Journal of Experimental Botany 65: 2937–2947.

Bowman, J.L. et al. (2017). Insights into land plant evolution garnered from the *Marchantia polymorpha* genome. Cell 171: 287-304.e15.

Briginshaw, L.N., Flores-Sandoval, E., Dierschke, T., Alvarez, J.P., and Bowman, J.L. (2022). KANADI promotes thallus differentiation and FR-induced gametangiophore formation in the liverwort Marchantia. New Phytologist 234: 1377–1393.

865 Cannell, N., Emms, D.M., Hetherington, A.J., MacKay, J., Kelly, S., Dolan, L., and Sweetlove,
866 L.J. (2020). Multiple Metabolic Innovations and Losses Are Associated with Major
867 Transitions in Land Plant Evolution. Current Biology 30: 1783-1800.e11.

868 Cao, J.-G., Wang, Q.-X., Zou, H.-M., Dai, X.-L., and Cao, T. (2013). New Observations on the
869 Morphology and Structure of *Marchantia polymorpha* Gametophores in Sexual
870 Reproduction Adaption. Plant Science Journal 31: 555.

871 Chiang, H.-H., Hwang, I., and Goodman, H.M. (1995). Isolation of the Arabidopsis *GA4* locus.
872 the Plant Cell 7: 195–201.

873 Chiyoda, S., Ishizaki, K., Kataoka, H., Yamato, K.T., and Kohchi, T. (2008). Direct transformation
874 of the liverwort Marchantia polymorpha L. by particle bombardment using immature thalli
875 developing from spores. Plant Cell Reports 27: 1467–1473.

876 Conesa, A. and Götz, S. (2008). Blast2GO: A comprehensive suite for functional analysis in
877 plant genomics. International Journal of Plant Genomics 2008.

878 Djakovic-Petrovic, T., Wit, M.D., Voesenek, L.A.C.J., and Pierik, R. (2007). DELLA protein
879 function in growth responses to canopy signals. Plant Journal 51: 117–126.

880 Downs, R.J., Hendricks, S.B., and Borthwick, H.A. (1957). Photoreversible Control of Elongation
881 of Pinto Beans and Other Plants under Normal Conditions of Growth. Botanical Gazette
882 118: 199–208.

883 Dubois, P.G., Olsefski, G.T., Flint-Garcia, S., Setter, T.L., Hoekenga, O.A., and Brutnell, T.P.
884 (2010). Physiological and Genetic Characterization of End-of-Day Far-Red Light
885 Response in Maize Seedlings. Plant Physiology 154: 173–186.

886 Fredericq, H. (1964). Influence formatrice de la lumière rouge-foncé sur le développement des
887 thalles de Marchantia polymorpha L. Bull. Soc. Roy. Bot. Belgique 98: 67–76.

888 Fredericq, H. and de Greef, J. (1966). Red (R), Far-red (FR) photoreversible control of growth
889 and chlorophyll content in light-grown thalli of Marchantia polymorpha L. Die
890 Naturwissenschaften 53: 337.

891 Fredericq, H. and Greef, J.D. (1968). Photomorphogenic and Chlorophyll Studies in the
892 Bryophyte Marchantia polymorpha. I. Effect of Red, Far-red Irradiations in Short and
893 Long-term Experiments. Physiol Plant 21: 346–359.

894 Gabriele, S., Rizza, A., Martone, J., Circelli, P., Costantino, P., and Vittorioso, P. (2009). The
895 Dof protein DAG1 mediates PIL5 activity on seed germination by negatively regulating
896 GA biosynthetic gene AtGA3ox1: DAG1 represses seed germination via PIL5 signalling.
897 The Plant Journal 61: 312–323.

898 Gamborg, O.L., Miller, R.A., and Ojima, K. (1968). Nutrient requirements of suspension cultures
899 of soybean root cells. Experimental Cell Research 50: 151–158.

García-Martínez, J.L., Keith, B., Bonner, B.A., Stafford, A.E., and Rappaport, L. (1987). Phytochrome Regulation of the Response to Exogenous Gibberellins by Epicotyls of *Vigna sinensis*. Plant Physiol. 85: 212–216.

Guindon, S., Dufayard, J.-F., Lefort, V., Anisimova, M., Hordijk, W., and Gascuel, O. (2010). New algorithms and methods to estimate maximum-likelihood phylogenies: Assessing the performance of PhyML 3.0. Systematic Biology 59: 307–321.

Hayashi, K., Horie, K., Hiwatashi, Y., Kawaide, H., Yamaguchi, S., Hanada, A., Nakashima, T., Nakajima, M., Mander, L.N., Yamane, H., Hasebe, M., and Nozaki, H. (2010). Endogenous diterpenes derived from *ent*-kaurene, a common gibberellin precursor, regulate protonema differentiation of the moss *Physcomitrella patens*. Plant Physiology 153: 1085–1097.

Hayashi, K. ichiro, Kawaide, H., Notomi, M., Sakigi, Y., Matsuo, A., and Nozaki, H. (2006). Identification and functional analysis of bifunctional *ent*-kaurene synthase from the moss *Physcomitrella patens*. FEBS Letters 580: 6175–6181.

Hedden, P. (2020). The Current Status of Research on Gibberellin Biosynthesis. Plant and Cell Physiology 61: 1832–1849.

Hedden, P., MacMillan, J., and Phinney, B.O. (1974). Fungal products. Part XII. Gibberellin A14-aldehyde, an intermediate in gibberellin biosynthesis in Gibberella fujikuroi. Journal of the Chemical Society, Perkin Transactions 1: 587–592.

Hellemans, J., Mortier, G., De Paepe, A., Speleman, F., and Vandesompele, J. (2008). qBase relative quantification framework and software for management and automated analysis of real-time quantitative PCR data. Genome Biology 8.

Helliwell, C.A., Chandler, P.M., Poole, A., Dennis, E.S., and Peacock, W.J. (2001a). The CYP88A cytochrome P450, *ent*-kaurenoic acid oxidase, catalyzes three steps of the gibberellin biosynthesis pathway. Proceedings of the National Academy of Sciences of the United States of America 98: 2065–2070.

Helliwell, C.A., Poole, A., James Peacock, W., and Dennis, E.S. (1999). Arabidopsis *ent* -kaurene oxidase catalyzes three steps of gibberellin biosynthesis. Plant Physiology 119: 507–510.

Helliwell, C.A., Sheldon, C.C., Olive, M.R., R.Walker, A., Zeevaart, J.A.D., Peacock, W.J., and Dennis, E.S. (1998). Cloning of the *Arabidopsis ent*-kaurene oxidase gene *GA3*. Proceedings of the National Academy of Sciences of the United States of America 95: 9019–9024.

Helliwell, C.A., Sullivan, J.A., Mould, R.M., Gray, J.C., James Peacock, W., and Dennis, E.S. (2001b). A plastid envelope location of *Arabidopsis ent*-kaurene oxidase links the plastid and endoplasmic reticulum steps of the gibberellin biosynthesis pathway. Plant Journal 28: 201–208.

937 Hernández-García, J., Sun, R., Serrano-Mislata, A., Inoue, K., Vargas-Chávez, C., Esteve-
938 Bruna, D., Arbona, V., Yamaoka, S., Nishihama, R., Kohchi, T., and Blázquez, M.A.
939 (2021). Coordination between growth and stress responses by DELLA in the liverwort
940 Marchantia polymorpha. Current Biology.

941 Hirano, K. et al. (2007). The GID1-mediated gibberellin perception mechanism is conserved in
942 the lycophyte Selaginella moellendorffii but not in the bryophyte *Physcomitrella patens*.
943 The Plant Cell 19: 3058–3079.

944 Hisamatsu, T., King, R.W., Helliwell, C. a, and Koshioka, M. (2005). The involvement of
945 gibberellin 20-oxidase genes in phytochrome-regulated petiole elongation of Arabidopsis.
946 Plant Physiology 138: 1106–1116.

947 Hisanaga, T., Okahashi, K., Yamaoka, S., Kajiwara, T., Nishihama, R., Shimamura, M., Yamato,
948 K.T., Bowman, J.L., Kohchi, T., and Nakajima, K. (2019). A cis -acting bidirectional
949 transcription switch controls sexual dimorphism in the liverwort. The EMBO Journal 38:
950 1–12.

951 Hoang, D.T., Chernomor, O., von Haeseler, A., Minh, B.Q., and Vinh, L.S. (2018). UFBoot2:
952 Improving the Ultrafast Bootstrap Approximation. Molecular Biology and Evolution 35:
953 518–522.

954 Holmes, M.G. and Smith, H. (1975). The function of phytochrome in plants growing in the natural
955 environment. Nature 254: 512–514.

956 Hornych, O., Testo, W.L., Sessa, E.B., Watkins, J.E., Campany, C.E., Pittermann, J., and Ekrt,
957 L. (2021). Insights into the evolutionary history and widespread occurrence of
958 antheridiogen systems in ferns. New Phytologist 229: 607–619.

959 Inoue, K., Nishihama, R., Araki, T., and Kohchi, T. (2019). Reproductive induction is a far-red
960 high irradiance response that is mediated by phytochrome and PHYTOCHROME
961 INTERACTING FACTOR in Marchantia polymorpha. Plant and Cell Physiology 60: 1136–
962 1145.

963 Inoue, K., Nishihama, R., Kataoka, H., Hosaka, M., Manabe, R., Nomoto, M., Tada, Y., Ishizaki,
964 K., and Kohchi, T. (2016). Phytochrome signaling is mediated by PHYTOCHROME
965 INTERACTING FACTOR in the liverwort *Marchantia polymorpha*. The Plant Cell 28:
966 1406–1421.

967 Ishizaki, K., Chiyoda, S., Yamato, K.T., and Kohchi, T. (2008). *Agrobacterium*-mediated
968 transformation of the haploid liverwort *Marchantia polymorpha* L., an emerging model for
969 plant biology. Plant and Cell Physiology 49: 1084–1091.

970 Ishizaki, K., Nishihama, R., Ueda, M., Inoue, K., Ishida, S., Nishimura, Y., Shikanai, T., and
971 Kohchi, T. (2015). Development of Gateway binary vector series with four different
972 selection markers for the liverwort *Marchantia polymorpha*. PLoS ONE 10: e0138876.

973 Iwasaki, M. et al. (2021). Identification of the sex-determining factor in the liverwort Marchantia
974 polymorpha reveals unique evolution of sex chromosomes in a haploid system. Current
975 Biology 31: 5522-5532.e7.

976 Jia, Q., Brown, R., Köllner, T.G., Fu, J., Chen, X., Wong, G.K.S., Gershenzon, J., Peters, R.J.,
977 and Chen, F. (2022). Origin and early evolution of the plant terpene synthase family.
978 Proceedings of the National Academy of Sciences of the United States of America 119:
979 1–9.

980 Kalyaanamoorthy, S., Minh, B.Q., Wong, T.K.F., von Haeseler, A., and Jermiin, L.S. (2017).
981 ModelFinder: fast model selection for accurate phylogenetic estimates. Nat Methods 14:
982 587–589.

983 Katoh, K. and Standley, D.M. (2013). MAFFT multiple sequence alignment software version 7:
984 Improvements in performance and usability. Molecular Biology and Evolution 30: 772–
985 780.

986 Katsumata, T., Hasegawa, A., Fujiwara, T., Komatsu, T., Notomi, M., Abe, H., Natsume, M., and
987 Kawaide, H. (2008). Arabidopsis CYP85A2 Catalyzes Lactonization Reactions in the
988 Biosynthesis of 2-Deoxy-7-oxalactone Brassinosteroids. Bioscience, Biotechnology, and
989 Biochemistry 72: 2110–2117.

990 Kohnen, M.V., Schmid-Siegert, E., Trevisan, M., Petrolati, L.A., Sénéchal, F., Müller-Moulé, P.,
991 Maloof, J., Xenarios, I., and Fankhauser, C. (2016). Neighbor Detection Induces Organ-
992 Specific Transcriptomes, Revealing Patterns Underlying Hypocotyl-Specific Growth.
993 Plant Cell 28: 2889–2904.

994 Koide, E., Suetsugu, N., Iwano, M., Gotoh, E., Nomura, Y., Stolze, S.C., Nakagami, H., Kohchi,
995 T., and Nishihama, R. (2020). Regulation of Photosynthetic Carbohydrate Metabolism by
996 a Raf-Like Kinase in the Liverwort Marchantia polymorpha. Plant and Cell Physiology 61:
997 631–643.

998 Koornneef, M. and van der Veen, J.H. (1980). Induction and analysis of gibberellin sensitive
999 mutants in *Arabidopsis thaliana* (L.) heynh. Theoretical and Applied Genetics 58: 257–
1000 263.

1001 Krijthe, J.H. (2015). Rtsne: T-Distributed Stochastic Neighbor Embedding using a Barnes-Hut
1002 Implementation.

1003 Kubota, A., Ishizaki, K., Hosaka, M., and Kohchi, T. (2013). Efficient *Agrobacterium*-mediated
1004 transformation of the liverwort *Marchantia polymorpha* using regenerating thalli.
1005 Bioscience, Biotechnology and Biochemistry 77: 167–172.

1006 Kumar, S. et al. (2016). Molecular diversity of terpene synthases in the liverwort *Marchantia*
1007 *polymorpha*. The Plant Cell 28: 2632–2650.

1008 Küpers, J.J. et al. (2023). Local light signaling at the leaf tip drives remote differential petiole
1009 growth through auxin-gibberellin dynamics. Current Biology 33: 75-85.e5.

1010 Kurihara, D., Mizuta, Y., Nagahara, S., and Higashiyama, T. (2021). ClearSeeAlpha: Advanced
1011 Optical Clearing for Whole-Plant Imaging. Plant and Cell Physiology 62: 1302–1310.

1012 Kurosawa, E. (1926). Experimental studies on the nature of the substance excreted by the
1013 "bakanae" fungus. Trans. Nat. Hist. Soc. Formosa 16: 213–227.

1014 Li, W., Liu, S.-W., Ma, J.-J., Liu, H.-M., Han, F.-X., Li, Y., and Niu, S.-H. (2020). Gibberellin
1015 Signaling Is Required for Far-Red Light-Induced Shoot Elongation in *Pinus tabuliformis*
1016 Seedlings. Plant Physiol. 182: 658–668.

1017 Love, M.I., Huber, W., and Anders, S. (2014). Moderated estimation of fold change and
1018 dispersion for RNA-seq data with DESeq2. Genome Biology 15: 550.

1019 Michaud, O., Krahmer, J., Galbier, F., Lagier, M., Galvão, V.C., Ince, Y.Ç., Trevisan, M., Knerova,
1020 J., Dickinson, P., Hibberd, J.M., Zeeman, S.C., and Fankhauser, C. (2023). Abscisic acid
1021 modulates neighbor proximity-induced leaf hyponasty in Arabidopsis. Plant Physiology
1022 191: 542–557.

1023 Minh, B.Q., Schmidt, H.A., Chernomor, O., Schrempf, D., Woodhams, M.D., von Haeseler, A.,
1024 and Lanfear, R. (2020). IQ-TREE 2: New Models and Efficient Methods for Phylogenetic
1025 Inference in the Genomic Era. Molecular Biology and Evolution 37: 1530–1534.

1026 Miyazaki, S., Hara, M., Ito, S., Tanaka, K., Asami, T., Hayashi, K., Kawaide, H., and Nakajima,
1027 M. (2018). An Ancestral Gibberellin in a Moss Physcomitrella patens. Molecular Plant 11:
1028 1097–1100.

1029 Miyazaki, S., Katsumata, T., Natsume, M., and Kawaide, H. (2011). The CYP701B1 of
1030 *Physcomitrella patens* is an ent-kaurene oxidase that resists inhibition by uniconazole-P.
1031 FEBS Letters 585: 1879–1883.

1032 Miyazaki, S., Nakajima, M., and Kawaide, H. (2015). Hormonal diterpenoids derived from ent-
1033 kaurenoic acid are involved in the blue-light avoidance response of Physcomitrella patens.
1034 Plant Signaling and Behavior 10: 1–4.

1035 Miyazaki, S., Toyoshima, H., Natsume, M., Nakajima, M., and Kawaide, H. (2014). Blue-light
1036 irradiation up-regulates the *ent*-kaurene synthase gene and affects the avoidance
1037 response of protonemal growth in *Physcomitrella patens*. Planta 240: 117–124.

1038 Morgan, D.C. and Smith, H. (1979). A systematic relationship between phytochrome-controlled
1039 development and species habitat, for plants grown in simulated natural radiation. Planta
1040 145: 253–258.

1041 Morgan, D.C. and Smith, H. (1978). The relationship between phytochrome-photoequilibrium
1042 and Development in light grown Chenopodium album L. Planta 142: 187–193.

1043 Motohashi, K. (2015). A simple and efficient seamless DNA cloning method using SLiCE from
1044 Escherichia coli laboratory strains and its application to SLiP site-directed mutagenesis.
1045 BMC Biotechnol 15: 47.

1046 Näf, U., Nakanishi, K., and Endo, M. (1975). On the Physiology and Chemistry of Fern
1047 Antheridiogens. Botanical Review 41: 315–359.

1048 Nelissen, H., Rymen, B., Jikumaru, Y., Demuynck, K., Van Lijsebettens, M., Kamiya, Y., Inzé,
1049 D., and Beemster, G.T.S. (2012). A Local Maximum in Gibberellin Levels Regulates
1050 Maize Leaf Growth by Spatial Control of Cell Division. Current Biology 22: 1183–1187.

1051 Ninnemann, H. and Halbsguth, W. (1965). Rolle des Phytochroms beim Etiolement von
1052 Marchantia polymorpha. Naturwissenschaften 52: 110–111.

1053 Nomura, T., Magome, H., Hanada, A., Takeda-Kamiya, N., Mander, L.N., Kamiya, Y., and
1054 Yamaguchi, S. (2013). Functional analysis of *Arabidopsis* CYP714A1 and CYP714A2
1055 reveals that they are distinct gibberellin modification enzymes. Plant and Cell Physiology
1056 54: 1837–1851.

1057 Ogawa, M., Hanada, A., Yamauchi, Y., Kuwahara, A., Kamiya, Y., and Yamaguchi, S. (2003).
1058 Gibberellin Biosynthesis and Response during Arabidopsis Seed Germination. The Plant
1059 Cell 15: 1591–1604.

1060 Patro, R., Duggal, G., Love, M.I., Irizarry, R.A., and Kingsford, C. (2017). Salmon provides fast
1061 and bias-aware quantification of transcript expression. Nature Methods 14: 417–419.

1062 Pluthero, F.G. (1993). Rapid purification of high-activity Taq DNA polymerase. Nucleic Acids
1063 Res 21: 4850–4851.

1064 Rojas, M.C., Hedden, P., Gaskin, P., and Tudzynski, B. (2001). The *P450–1* gene of *Gibberella*
1065 *fujikuroi* encodes a multifunctional enzyme in gibberellin biosynthesis. Proc. Natl. Acad.
1066 Sci. U.S.A. 98: 5838–5843.

1067 Sakamoto, Y., Ishimoto, A., Sakai, Y., Sato, M., Nishihama, R., Abe, K., Sano, Y., Furuichi, T.,
1068 Tsuji, H., Kohchi, T., and Matsunaga, S. (2022). Improved clearing method contributes to
1069 deep imaging of plant organs. Commun Biol 5: 12.

1070 Schindelin, J. et al. (2012). Fiji: an open-source platform for biological-image analysis. Nat
1071 Methods 9: 676–682.

1072 Schmidt, U., Weigert, M., Broaddus, C., and Myers, G. (2018). Cell Detection with Star-Convex
1073 Polygons. In Medical Image Computing and Computer Assisted Intervention – MICCAI
1074 2018, A.F. Frangi, J.A. Schnabel, C. Davatzikos, C. Alberola-López, and G. Fichtinger,
1075 eds, Lecture Notes in Computer Science. (Springer International Publishing: Cham), pp.
1076 265–273.

1077 Schneller, J.J. (2008). Antheridiogens. In Biology and Evolution of Ferns and Lycophytes, T.A.
1078 Ranker and C.H. Haufler, eds (Cambridge University Press: New York), pp. 134–158.

1079 Sessa, G., Carabelli, M., Sassi, M., Ciolfi, A., Possenti, M., Mittempergher, F., Becker, J., Morelli,
1080 G., and Ruberti, I. (2005). A dynamic balance between gene activation and repression
1081 regulates the shade avoidance response in *Arabidopsis*. Genes Dev. 19: 2811–2815.

1082 Shimamura, M. (2016). *Marchantia polymorpha*: Taxonomy, phylogeny and morphology of a
1083 model system. Plant and Cell Physiology 57: 230–256.

1084 Sponsel, V.M. (2016). Signal achievements in gibberellin research: the second half-century.
1085 Annual Plant Reviews: The Gibberellins 49: 1–36.

1086 Streubel, S., Deiber, S., Rötzer, J., Mosiolek, M., Jandrasits, K., and Dolan, L. (2023). Meristem
1087 dormancy in Marchantia polymorpha is regulated by a liverwort-specific miRNA and a
1088 clade III SPL gene. Current Biology: S0960982222019996.

1089 Sugano, S.S., Nishihama, R., Shirakawa, M., Takagi, J., Matsuda, Y., Ishida, S., Shimada, T.,
1090 Hara-Nishimura, I., Osakabe, K., and Kohchi, T. (2018). Efficient CRISPR/Cas9-based
1091 genome editing and its application to conditional genetic analysis in Marchantia
1092 polymorpha. PLoS ONE 13: e0205117.

1093 Sun, T. and Kamiya, Y. (1994). The Arabidopsis *GA1* locus encodes the cyclase *ent*-kaurene
1094 synthetase A of gibberellin biosynthesis. the Plant Cell 6: 1509–1518.

1095 Talon, M., Koornneef, M., and Zeevaart, J.A.D. (1990). Endogenous gibberellins in Arabidopsis
1096 thaliana and possible steps blocked in the biosynthetic pathways of the semidwarf ga4
1097 and ga5 mutants. Proceedings of the National Academy of Sciences of the United States
1098 of America 87: 7983–7987.

1099 Tanaka, J., Yano, K., Aya, K., Hirano, K., Takehara, S., Koketsu, E., Ordonio, R.L., Park, S.-H.,
1100 Nakajima, M., Ueguchi-Tanaka, M., and Matsuoka, M. (2014). Antheridiogen determines
1101 sex in ferns via a spatiotemporally split gibberellin synthesis pathway. Science 346: 469–
1102 473.

1103 Toyomasu, T., Kawaide, H., Mitsuhashi, W., Inoue, Y., and Kamiya, Y. (1998). Phytochrome
1104 regulates gibberellin biosynthesis during germination of photoblastic lettuce seeds. Plant
1105 Physiology 118: 1517–1523.

1106 Ubeda-Tomás, S., Federici, F., Casimiro, I., Beemster, G.T.S., Bhalerao, R., Swarup, R.,
1107 Doerner, P., Haseloff, J., and Bennett, M.J. (2009). Gibberellin Signaling in the
1108 Endodermis Controls Arabidopsis Root Meristem Size. Current Biology 19: 1194–1199.

1109 Ubeda-Tomás, S., Swarup, R., Coates, J., Swarup, K., Laplaze, L., Beemster, G.T.S., Hedden,
1110 P., Bhalerao, R., and Bennett, M.J. (2008). Root growth in Arabidopsis requires
1111 gibberellin/DELLA signalling in the endodermis. Nat Cell Biol 10: 625–628.

1112 Urrutia, O., Hedden, P., and Rojas, M.C. (2001). Monooxygenases involved in GA12 and GA14
1113 synthesis in Gibberella fujikuroi. Phytochemistry 56: 505–511.

1114 Van Tuinen, A., Peters, A.H.L.J., Kendrick, R.E., Zeevaart, J. a. D., and Koornneef, M. (1999).
1115 Characterisation of the procera mutant of tomato and the interaction of gibberellins with
1116 end-of-day far-red light treatments. Physiologia Plantarum 106: 121–128.

1117 Wenzel, C.L., Williamson, R.E., and Wasteneys, G.O. (2000). Gibberellin-Induced Changes in
1118 Growth Anisotropy Precede Gibberellin-Dependent Changes in Cortical Microtubule
1119 Orientation in Developing Epidermal Cells of Barley Leaves. Kinematic and Cytological
1120 Studies on a Gibberellin-Responsive Dwarf Mutant, M489. Plant Physiology 124: 813–
1121 822.

1122 Whitelam, G.C. and Johnson, C.B. (1982). PHOTOMORPHOGENESIS IN IMPATIENS
1123 PARVIFLORA AND OTHER PLANT SPECIES UNDER SIMULATED NATURAL
1124 CANOPY RADIATIONS. New Phytol 90: 611–618.

1125 Whitelam, G.C. and Smith, H. (1991). Retention of Phytochrome-Mediated Shade Avoidance
1126 Responses in Phytochrome-Deficient Mutants of Arabidopsis, Cucumber and Tomato.
1127 Journal of Plant Physiology 139: 119–125.

1128 Williams, J., Phillips, A.L., Gaskin, P., and Hedden, P. (1998). Function and Substrate Specificity
1129 of the Gibberellin 3β-Hydroxylase Encoded by the Arabidopsis GA4Gene. Plant
1130 Physiology 117: 559–563.

1131 Xu, S., Li, L., Luo, X., Chen, M., Tang, W., Zhan, L., Dai, Z., Lam, T.T., Guan, Y., and Yu, G.
1132 (2022). Ggtree: A serialized data object for visualization of a phylogenetic tree and
1133 annotation data. iMeta 1: e56.

1134 Yamaguchi, S., Smith, M.W., Brown, R.G.S., Kamiya, Y., and Sun Tai-ping (1998a).
1135 Phytochrome Regulation and Differential Expression of Gibberellin 3β-Hydroxylase
1136 Genes in Germinating Arabidopsis Seeds. The Plant Cell 10: 2115–2126.

1137 Yamaguchi, S., Sun, T., Kawaide, H., and Kamiya, Y. (1998b). The *GA2* locus of *Arabidopsis*
1138 *thaliana* encodes *ent*-kaurene synthase of gibberellin biosynthesis. Plant Physiology 116:
1139 1271–1278.

1140 Yamane, H. (1998). Fern Antheridiogens. International Review of Cytology 184: 1–32.

1141 Yamaoka, S. et al. (2018). Generative Cell Specification Requires Transcription Factors
1142 Evolutionarily Conserved in Land Plants. Current Biology 28: 479-486.e5.

1143 Yamauchi, T., Oyama, N., Yamane, H., Murofushi, N., Schraudolf, H., Pour, M., Furber, M., and
1144 Mander, L.N. (1996). Identification of Antheridiogens in Lygodium circinnatum and
1145 Lygodium flexuosum. Plant Physiology 111: 741–745.

1146 Yoshida, H., Takehara, S., Mori, M., Ordonio, R.L., and Matsuoka, M. (2020). Evolution of GA
1147 metabolic enzymes in land plants. Plant and Cell Physiology 61: 1919–1934.

1148 Yu, G. (2022). Data Integration, Manipulation and Visualization of Phylogenetic Trees (Chapman
1149 and Hall/CRC: New York).

1150 Yu, G. (2020a). Gene ontology semantic similarity analysis using GOSemSim. In Methods in
1151 Molecular Biology (Humana Press Inc.), pp. 207–215.

1152 Yu, G. (2020b). Using ggtree to Visualize Data on Tree-Like Structures. Current Protocols in
1153 Bioinformatics 69: e96.

1154 Yu, G., Lam, T.T.-Y., Zhu, H., and Guan, Y. (2018). Two Methods for Mapping and Visualizing
1155 Associated Data on Phylogeny Using Ggtree. Molecular Biology and Evolution 35: 3041–
1156 3043.

1157 Yu, G., Li, F., Qin, Y., Bo, X., Wu, Y., and Wang, S. (2010). GOSemSim: an R package for
1158 measuring semantic similarity among GO terms and gene products. Bioinformatics 26:
1159 976–978.

1160 Yu, G., Smith, D.K., Zhu, H., Guan, Y., and Lam, T.T.-Y. (2017). ggtree: an r package for
1161 visualization and annotation of phylogenetic trees with their covariates and other
1162 associated data. Methods in Ecology and Evolution 8: 28–36.

1163 Zhang, Y., Werling, U., and Edelmann, W. (2012). SLiCE: A novel bacterial cell extract-based
1164 DNA cloning method. Nucleic Acids Research 40: 1–10.

1165

1166

Main Figures

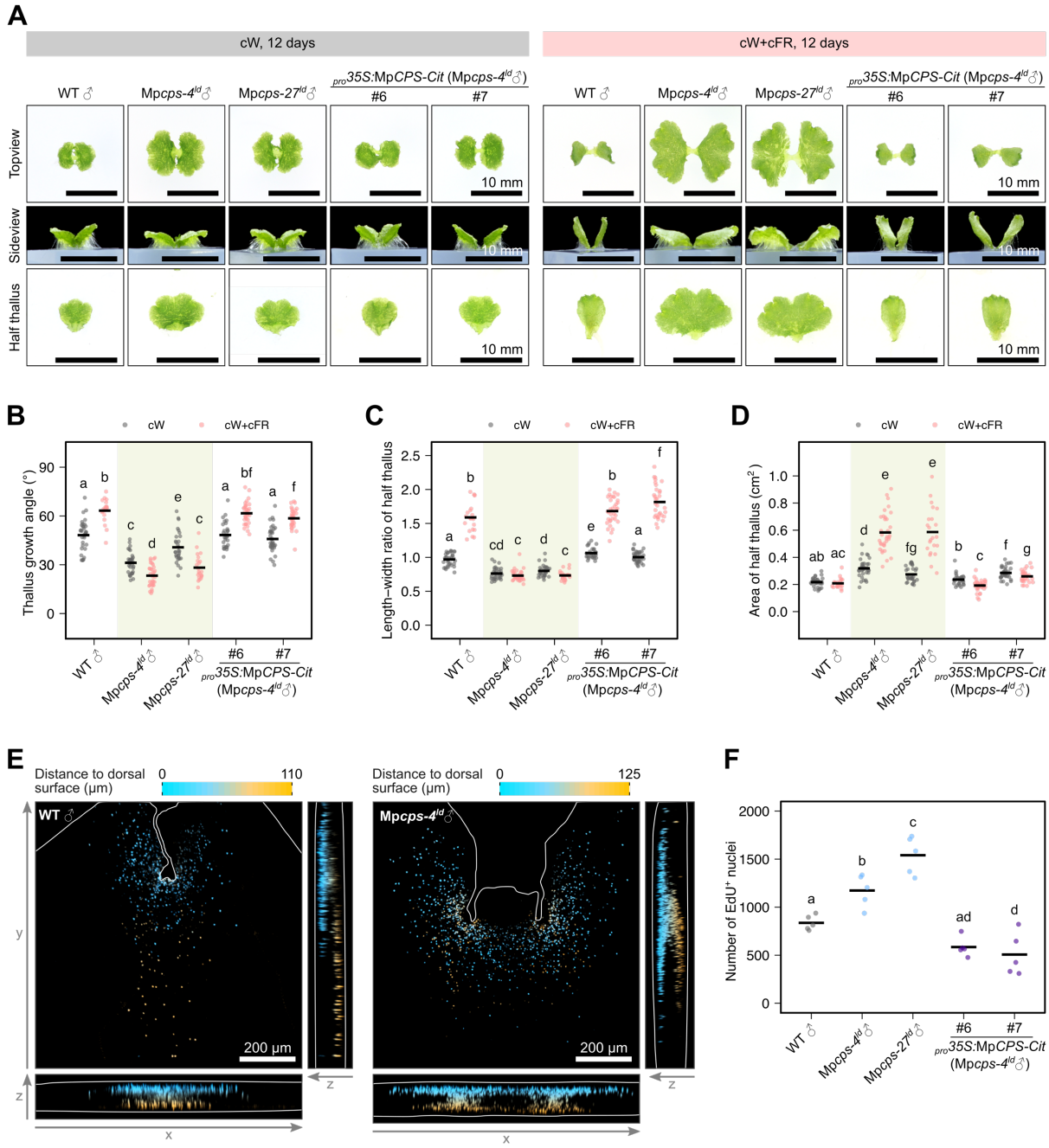

Figure 1 Loss of Mp*CPS* activity alters thallus morphology under far-red light (FR) enriched conditions. A, Morphology of 12-day-old plants grown from gemmae under continuous white light (cW) or continuous white light with far-red light (cW+cFR) conditions. Images were selected randomly from different plants. Bars = 10 mm. B-D, Measurements of the thallus growth angle (B), length-width ratio (C) and thallus area (D) from half plants shown in A. n=21-36. E, Apical regions of plants labelled with 5-ethynyl-2'-deoxyuridine (EdU) after 7-day growth in cW+cFR, showing two-dimensional projections of color-coded z-stacks. White lines mark the boundary of plants or imaging area. F, Number of nuclei with positive EdU signals in the apical regions of 7-day-old plants grown in cW+cFR (n=5). For all figures, WT♂ refer to Tak-1 wild-type plants. For B-D and F, each dot represents data from a "half thallus", which was developed from a single meristem of the gemma. Horizontal lines represent mean values. Letters represent statistical differences, and groups with no common letters were significantly different (adjusted $p<0.05$). For B-D, non-pooled Welch's *t*-test with Benjamini-Hochberg (B-H) adjustment was used due to heterogeneity of variance. Tukey's HSD test was used in F.

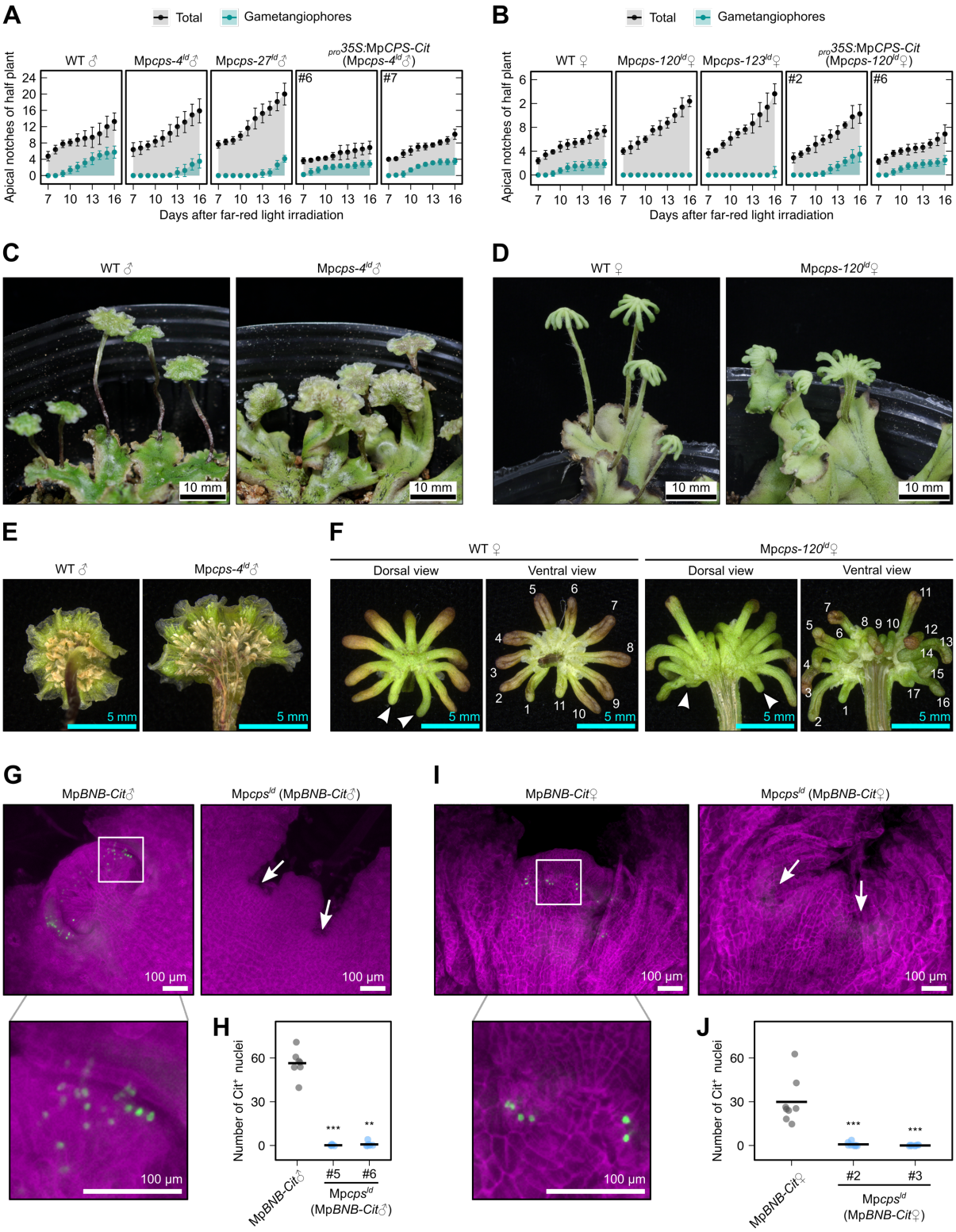
A
Total
Gametangiophores
WT ♂
Mpcps-4ld♂
Mpcps-27ld♂
proMp35S:MpCPS-Cit (Mpcps-4ld♂)
#6
#7
Apical notches of half plant
Days after far-red light irradiation
B
WT ♀
Mpcps-120ld♀
Mpcps-123ld♀
proMp35S:MpCPS-Cit (Mpcps-120ld♀)
#2
#6
C
WT ♂
Mpcps-4ld♂
10 mm
D
WT ♀
Mpcps-120ld♀
10 mm
E
WT ♂
Mpcps-4ld♂
5 mm
F
WT ♀
Mpcps-120ld♀
Dorsal view
Ventral view
5 mm
G
MpBNB-Cit♂
Mpcpsld (MpBNB-Cit♂)
100 µm
H
Number of Cit+ nuclei
MpBNB-Cit♂
#5
#6
Mpcpsld (MpBNB-Cit♂)
I
MpBNB-Cit♀
Mpcpsld (MpBNB-Cit♀)
J
MpBNB-Cit♀
#2
#3
Mpcpsld (MpBNB-Cit♀)

Figure 2 Mp*CPS* is required for delayed sexual reproduction and affected gametangiophore morphology.

A-B, Progress of apical bifurcation and gametangiophore formation in male (A) and female (B) plants, which were cultured aseptically under cW for 7 days before transferred to cW+cFR. Dots and error bars represent means and standard deviations, respectively. n=8. WT♂ and WT♀ refer to Tak-1 and Tak-2 wild-type plants, respectively. C-D, Photos of male (C) and female (D) plants bearing gametangiophores, cultured on vermiculite under cW+cFR from thallus fragments for 81 and 63 days, respectively. E, Ventral view of antheridiophores. F, Dorsal and ventral view of archegoniophores. Arrowheads indicate marginal digitate rays, and the number of digitate rays was labeled in the ventral view. G-J, Fluorescence microscopic images and quantification of MpBNB-Cit accumulation in the apical regions of 11-day-old male (G-H, dorsal view), or 14-day-old female (I-J, ventral view) plants cultured under cW+cFR from gemmae. G and I, Z-projections of image stacks, with cell walls stained with calcofluor white (purple) and Citrine signals shown in green. Arrows indicate apical meristems. H and J, Number of Citrine-positive nuclei counted from projection of image stacks. Each dot represents data from 1/2 (H) or 1/4 (J) of the thallus, and horizontal lines represent mean values. Asterisks show statistical difference compared to the control group (Mann-Whitney *U* test; **, $p<0.01$; ***, $p<0.001$). n=7 for H, n=8 for J.

A

Metabolite	Endogenous Level	Metabolite	Endogenous Level
GA_1	not detected	GA_{20}	not detected
GA_4	not detected	GA_{24}	not detected
GA_8	not detected	GA_{29}	not detected
GA_9	not detected	GA_{34}	not detected
GA_{12}	28.9±6.5	GA_{44}	not detected
GA_{15}	not detected	GA_{51}	not detected
GA_{19}	not detected	GA_{53}	not detected

(unit: pg/g fresh weight)

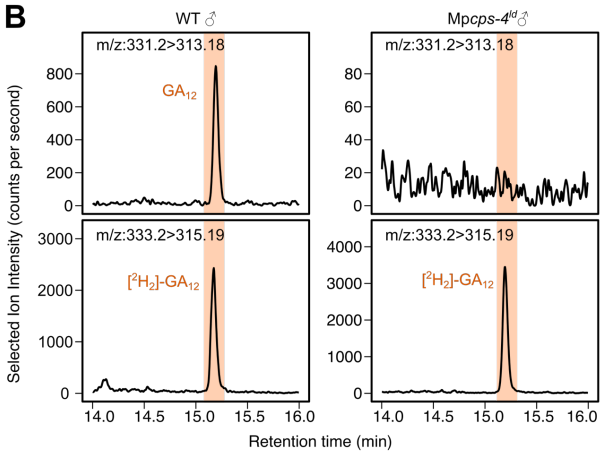

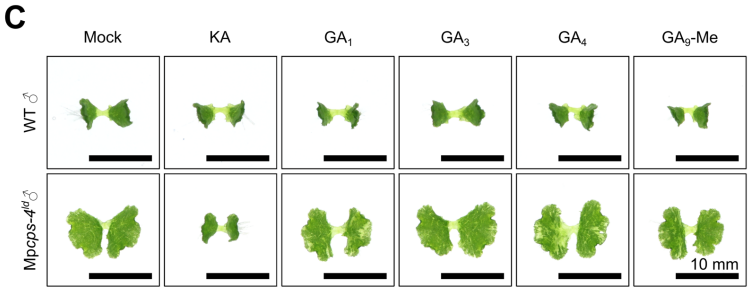

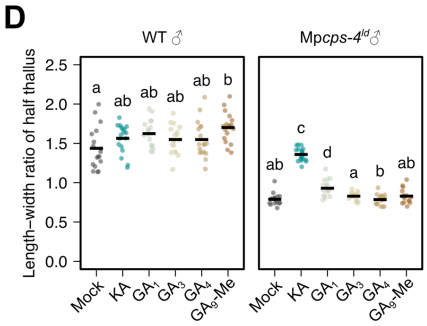

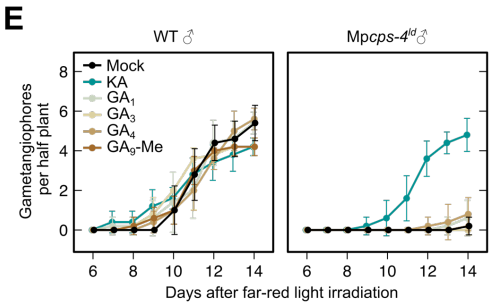

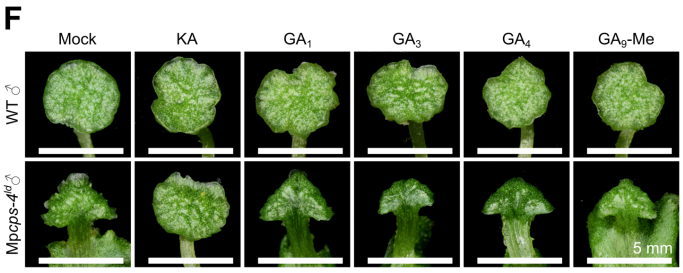

Figure 3 Endogenous levels of and responsiveness to KA or GAs in wild-type and Mp*cps*^{ld} plants.
A, Endogenous levels of GAs measured in wild-type plants (Tak-1) by LC-MS/MS. B, Selected ion chromatography showing peak of endogenous GA_{12} in comparison with the $^{2}H_{2}$-labeled internal standard. For A-B, plants were cultured under cW for 10 days, then induced under cW+cFR for 3 days. C-D, Effect of 2-μM KA or GAs on the morphology of 12-day-old thalli cultured under cW+cFR from gemmae. Horizontal bars in D represent mean values, and letters represent multiple comparisons with non-pooled Welch's *t*-test and B-H adjustment (adjusted $p<0.05$ for non-overlapping letters, n=16-18). E-F, Effect of 2-μM KA or GAs on gametangiophore formation (E) and morphology (F). Plants were cultured aseptically under cW for 7 days before transferred to cW+cFR. Dots and error bars represent mean±SD in E (n=5). Bars = 10 mm in C and 5 mm in F.

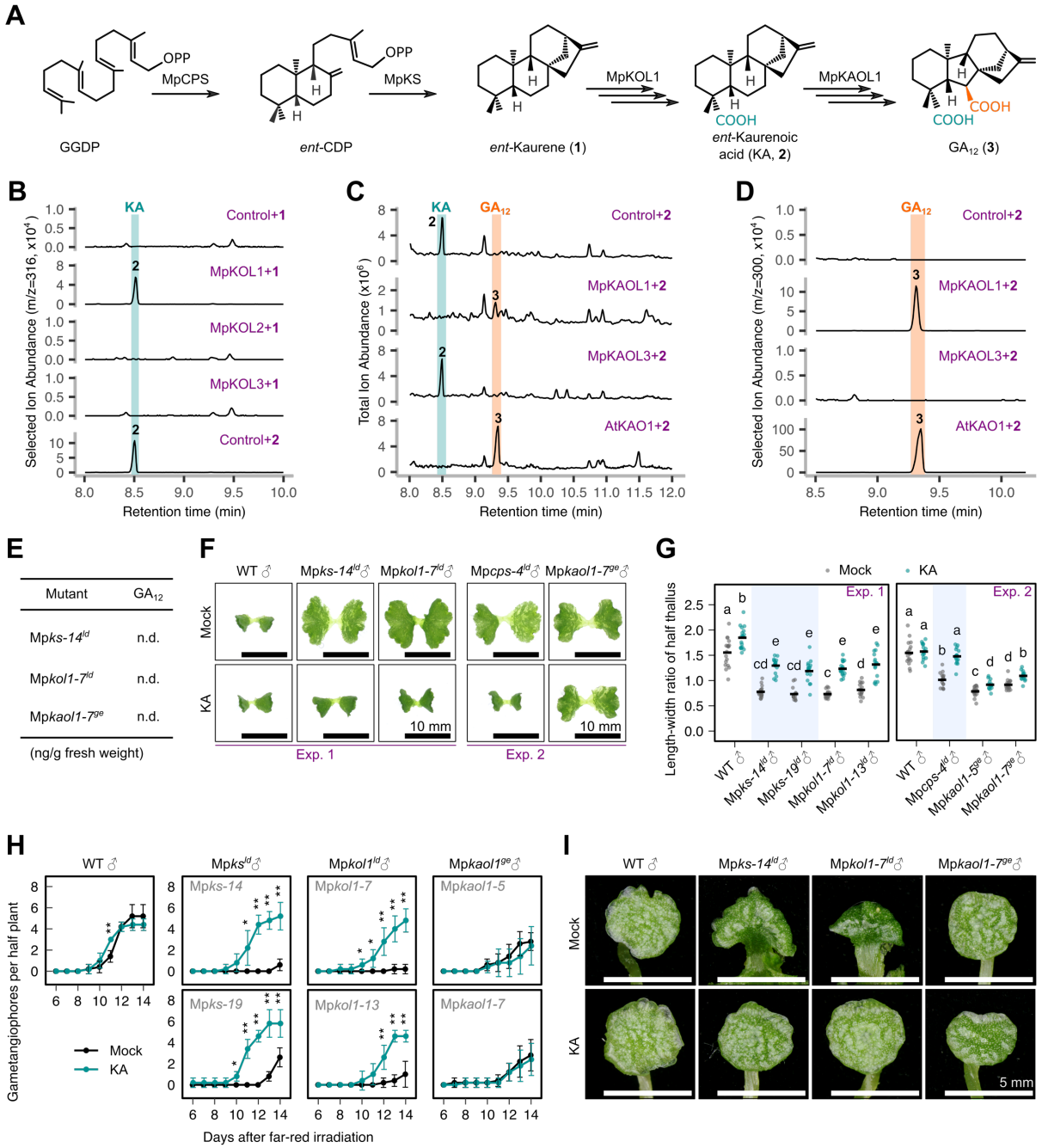
A
OPP
MpCPS
OPP
MpKS
MpKOL1
MpKAOL1
COOH
COOH
COOH
GGDP
ent-CDP
ent-Kaurene (1)
ent-Kaurenoic acid (KA, 2)
GA12 (3)
B
KA
Control+1
MpKOL1+1
MpKOL2+1
MpKOL3+1
Control+2
Selected Ion Abundance (m/z=316, x10^4)
Retention time (min)
C
KA
GA12
Control+2
MpKAOL1+2
MpKAOL3+2
AtKAO1+2
Total Ion Abundance (x10^6)
Retention time (min)
D
GA12
Control+2
MpKAOL1+2
MpKAOL3+2
AtKAO1+2
Selected Ion Abundance (m/z=300, x10^4)
Retention time (min)
E
Mutant
GA12
Mpks-14ld
n.d.
Mpkol1-7ld
n.d.
Mpkaol1-7ge
n.d.
(ng/g fresh weight)
F
WT ♂
Mpks-14ld♂
Mpkol1-7ld♂
Mpcps-4ld♂
Mpkaol1-7ge♂
Mock
KA
10 mm
10 mm
Exp. 1
Exp. 2
G
Mock
KA
Exp. 1
Exp. 2
Length-width ratio of half thallus
WT ♂
Mpks-14ld♂
Mpks-19ld♂
Mpkol1-7ld♂
Mpkol1-13ld♂
WT ♂
Mpcps-4ld♂
Mpkaol1-5ge♂
Mpkaol1-7ge♂
H
WT ♂
Mpksld♂
Mpkol1ld♂
Mpkaol1ge♂
Mpks-14
Mpks-19
Mpkol1-7
Mpkol1-13
Mpkaol1-5
Mpkaol1-7
Gametangiophores per half plant
Mock
KA
Days after far-red irradiation
I
WT ♂
Mpks-14ld♂
Mpkol1-7ld♂
Mpkaol1-7ge♂
Mock
KA
5 mm

Figure 4 Biosynthetic route for GA_{12} production in *M. polymorpha*.
A, Proposed enzymatic steps for GA_{12} biosynthesis in *M. poymorpha*. B-D, GC-MS analysis showing conversion of *ent*-kaurene to KA (B), and KA to GA_{12} (C-D) by yeast cultures expressing KO and KAO homologs. E, biosynthesis mutants with GA_{12} below the detection limit. n.d., not detected. F-G, morphlogy of 12-day-old mutants grown under cW+cFR with or without 2 μM KA. Horizontal bars in G represent mean values, and letters represent multiple comparisons with non-pooled Welch's *t*-test and B-H adjustment (adjusted $p<0.05$ for non-overlapping letters, n=14-18). H-I, Gametangiophore formation progress (H) and morphology (I) of mutants, cultured aseptically under cW for 7 days before transferred to cW+cFR and treated with 2 μM KA. Dots and error bars represent mean±SD in H (n=5). Bars = 10 mm in F and 5 mm in I.

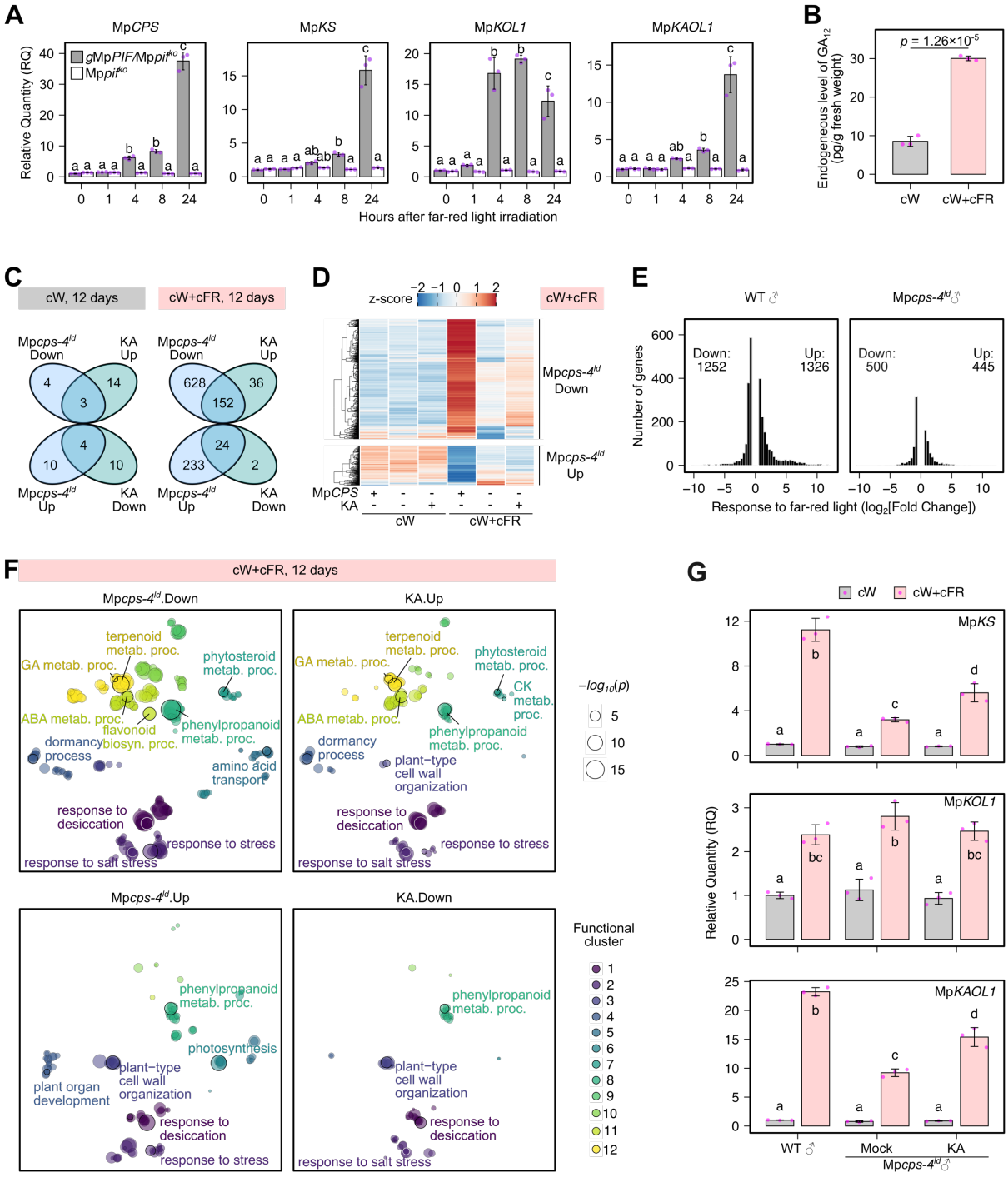
A
MpCPS
MpKS
MpKOL1
MpKAOL1
Relative Quantity (RQ)
gMpPIF/Mppif^ko
Mppif^ko
Hours after far-red light irradiation
B
Endogeneous level of GA12 (pg/g fresh weight)
p = 1.26×10^-5
cW
cW+cFR
C
cW, 12 days
cW+cFR, 12 days
Mpcps-4^ld Down
KA Up
Mpcps-4^ld Up
KA Down
D
z-score
cW+cFR
Mpcps-4^ld Down
Mpcps-4^ld Up
MpCPS
KA
cW
cW+cFR
E
WT ♂
Mpcps-4^ld ♂
Number of genes
Down: 1252
Up: 1326
Down: 500
Up: 445
Response to far-red light (log2[Fold Change])
F
cW+cFR, 12 days
Mpcps-4^ld.Down
KA.Up
Mpcps-4^ld.Up
KA.Down
terpenoid metab. proc.
phytosteroid metab. proc.
GA metab. proc.
ABA metab. proc.
flavonoid biosyn. proc.
phenylpropanoid metab. proc.
dormancy process
amino acid transport
CK metab. proc.
plant-type cell wall organization
response to desiccation
response to stress
response to salt stress
photosynthesis
plant organ development
−log10(p)
Functional cluster
G
cW
cW+cFR
MpKS
MpKOL1
MpKAOL1
Relative Quantity (RQ)
WT ♂
Mock
KA
Mpcps-4^ld ♂

Figure 5 Transcriptional regulation related to GA biosynthesis in *M. polymorpha*.
A, Relative expression level of GA biosynthesis genes by qPCR in Mp*pif*^{ko} and its complementation line, cultured under cW for 7 days and then transferred to cW+cFR. B, endogenous level of GA_{12} in Tak-1 plants cultured under cW for 10 days, then under cW or cW+cFR for 4 days. The data for cW+cFR group is the same as in Figure 3A. The *p*-value was calculated by Student's *t*-test. C, Number of differentially expressed genes (DEGs) between 12-day-old Mp*cps*^{ld} and Tak-1 plants, or Mp*cps-4*^{ld} plants grown with or without 2-μM KA under indicated light conditions (Wald test with B-H adjustment by DESeq2, DEG defined as adjusted $p<0.01$ and $|\log_2(\text{Fold Change})|>0.585$). D, expression patterns of up- and down-regulated genes in Mp*cps-4*^{ld}. E, Distribution of DEGs induced by FR enrichment in Tak-1 and Mp*cps-4*^{ld} plants, comparing transcriptomes of cW+cFR to cW conditions. F, GO term enrichment analysis of DEG sets shown in (C). Each dot shows a significant enriched biological process term ($p<0.01$ by Fisher's exact test), and semantically similar terms were plotted in color-coded clusters. Selected terms were highlighted with annotations. metab. proc., metabolic process. See Supplemental Data Set 2 for full lists. G, Relative expression level of GA biosynthesis genes by qPCR in plants cultured under cW for 11 days, then transferred to cW+cFR with or without 2-μM KA treatment. All bar plots with error bars (A-B, G) represent mean±SD from 3 biological replicates. Letters in A and G represent multiple comparisons with Tukey's HSD test (adjusted $p<0.05$ for non-overlapping letters).